JMEPEG (2023) 32:10637–10654
https://doi.org/10.1007/s11665-023-08322-5

©ASM International
1059-9495/$19.00

TECHNICAL ARTICLE

Assessing the Surface Properties of Plant Extract-Based Silver Nanoparticle Coatings on 17–4 PH Stainless Steel Foams Using Artificial Intelligence-Supported RGB Analysis: A Comparative Study

Nuray Beköz Üllen, Gizem Karabulut, and Selcan Karakuş

Submitted: 21 February 2023 / Revised: 3 May 2023 / Accepted: 7 May 2023 / Published online: 19 May 2023

17–4 PH Stainless Steel Foam (SSF) is widely used in biomedical implants due to its low cost, high mechanical properties, good corrosion resistance, and biocompatibility. In order to expand its applicability in the near future, it is necessary to improve the surface properties of the porous structure. This study primarily focuses on the surface modification of SSF with silver nanoparticles (Ag NPs) synthesized from various plant extracts and their superficial characterization. The Ag NPs were synthesized with extracts from some plants such as locust bean gum, matcha tea, and maca root by a sonochemical method, and their morphology, crystal structure, and chemical functional groups were characterized. The different matrix-based Ag NPs were then coated on 17–4 PH SSF, which has irregularly shaped pores and a porosity of approximately 70%, using the drop-casting method. To understand the effects of different matrix-based Ag NPs coatings on the surface characteristics of the porous structure, versatile investigations were carried out using traditional and digital image-based methods. While the structural and surface properties of the SSFs changed after nanocoating, they showed similar properties when the different matrix-based Ag NPs were used. The RGB analysis results and opacity values showed differences depending on the coating solution obtained from different plant extracts. Overall, the results illustrate the importance of surface nanomodification of the different matrix-based Ag NPs-coated 17–4 PH SSF to achieve favorable surface performance to obtain promising multifunctional nanoplatforms for biomedical applications.

Keywords Ag NPs, green industry, nanomaterials, opacity, porous materials, RGB analysis, surface modification

1. Introduction

Metallic foams have recently garnered significant attention in both academia and industry due to of their low specific weights, good physical properties, and high energy absorption capacity, high stiffness, high damping capacity, good vibration damping characteristics, and excellent thermal properties (Ref 1-4). Among these, 17–4 PH SSF offers advantages such as low cost, high porosity, impact strength, tensile strength, fracture toughness, and good corrosion resistance making them widely used in various fields, including thermal and sound insulation, energy absorption, heat exchange, filtration, lightweight construction, and biomedical implants (Ref 5, 6). Metallic foams, such as 17–4 PH SSF, hold significant potential in bone-related implant applications, aerospace applications, chemical, and food processing industries due to their porous structure (Ref 7). The properties required for implant materials are biocompatibility, corrosion and abrasion resistance, low density, open porosity, mechanical strength close to the cancellous bone, and commercialization potential. For this reason, a comprehensive understanding of not only the microstructure and mechanical properties but also the superficial properties are necessary for a successful implementation in biomedical applications. Although there has been considerable research on steel foam focused on its mechanical and chemical properties (Ref 5, 8-11), studies on the characterization of superficial properties are still lacking in the literature. The material surface in implant applications is exposed to various material degradations, such as corrosion, oxidation, wear, and fatigue, which typically begin at the surface. Therefore, the surface quality of metallic materials used in biomedical implants is critical to their service performance. The success of implementing the 17-4PH SSF is largely dependent on optimizing the surface coating technology to improve microstructures and mechanical properties.

The reliability of the implant depends largely on its surface layer's physical condition, as the surface properties directly affect the expectations of biomedical implants. For this reason, surface modifications play an important role in the production stage to improve the functional performance and biocompatibility of metallic foam implants. Coating is a popular surface modification method used to impart functional properties such as corrosion protection, antibacterial, and non-wettability to both dense and porous materials. The biocompatibility of

Nuray Beköz Üllen and **Gizem Karabulut**, Faculty of Engineering, Department of Metallurgical and Material Engineering, Istanbul University-Cerrahpaşa, Istanbul, Turkey; and **Selcan Karakuş**, Faculty of Engineering, Department of Chemistry, Istanbul University-Cerrahpaşa, Istanbul, Turkey. Contact e-mails: nbekoz@iuc.edu.tr and selcan@iuc.edu.tr.

porous metallic foams can be further improved by using various multifunctional coatings (Ref 12-15). However, there is only one study reported on the coating of 17–4 PH SSF in the literature. In the study by Karakuş et al. (Ref 16), 17–4 PH stainless steel was coated with CMC/Chitosan-α-Fe_2O_3 NPs, and characterized. There are not enough studies on the coatability and surface properties of steel foams. Therefore, these characteristics need to be examined further to use 17–4 PH SSF material on a large scale. The main objective of this study is to investigate the superficial properties of the surface-modified 17–4 PH SSF with different matrix-based Ag NPs in detail. The synthesis of metal-based NPs is achieved through various physical and chemical methods, including electrochemical reduction (Ref 17), wet chemical (Ref 18), steam, photochemical reduction methods, etc. (Ref 19). While these techniques have proven successfully in synthesizing NPs, they are often expensive and often contain harmful chemicals (Ref 20). Due to an increasing interest in green chemistry and other biological processes, scientists have sought environmentally friendly approaches for NP synthesis (Ref 21-25). Nowadays, the green sonochemical method has become a frequently used method due to its simplicity, economy, lack of toxic substances, suitability for pharmacological and biomedical applications, and ability to facilitate commercial production in a wide range (Ref 26). Among all kinds of nano-engineered metallic NPs, Ag NPs have received increasing attention due to their unique physical, chemical, and biological properties compared to their macroscale form (Ref 27-29). Ag NPs have distinctive physicochemical properties such as high electrical and thermal conductivity, high specific surface area, high mechanical strength, catalytic activity, and plasmon-resonance optical scattering (Ref 29-31). These properties make Ag NPs important in industries such as textiles, chemistry, and cosmetics, as well as in biomedical applications such as microelectronics, drug carriers, medical imaging, and coatings in implants (Ref 32-36). Ag NPs are important for the surface coating of metallic implant materials as they prevent bacterial adhesion to the surface and improve corrosion resistance (Ref 37, 38). Sharonova et al. stated that the surface charge variation properties of Ag NPs also significantly affect the properties of the surface, especially in coating applications (REF 39). Stabilizers are extremely important in order to manage these physicochemical properties of the Ag NPs at the nanoscale (Ref 40). Polymers and surfactants are commonly used as stabilizers to obtain stable nanoformulations (Ref 41). Recently, plant-based stabilization has come to the fore in nanotechnology studies (Ref 28, 29, 42, 43). In this study, one of the main objectives is to produce Ag NPs in different matrixes (maca root, matcha tea, and locust bean gum extracts) and to examine the effect of surface properties in the nanocoating process. Maca (Mac) is a type of plant that has been used for about 2000 years by people and is known as a medicinal plant (Ref 44). Matcha (Mat) is a green tea in powdered form. The high levels of phenolic compounds in its content cause it to show antioxidant properties (Ref 45, 46). Locust bean gum (Loc) is a natural polymer and is used in various sectors, especially in the pharmaceutical and food sectors, due to its biocompatibility, adhesiveness, edibility, and thickening properties (Ref 37). Thus, all stabilizers used in this study are fully biocompatible and biodegradable. In our previous study (Ref 37), 316L stainless steel was coated with organic locust gum/polyethylene glycol silver nanoparticles (Loc/PEG-Ag NPs), and found that the antibacterial and anticorrosive performance of surface-modified dense SS316L was improved. As Ag NPs are known to have antibacterial properties, in this study, Ag NPs prepared with different matrices were coated on 17–4 PH SSF for the first time, and their superficial properties were compared.

This study comprises of four main steps: (1) Synthesizing Ag NPs with different matrices using a green and inexpensive sonochemical method. (2) Characterizing the morphology, crystal structure, and chemical functional groups of the synthesized Ag NPs. (3) Coating 17–4 PH SSFs with high porosity with the synthesized Ag NPs using the drop-casting method. (4) Comparatively characterizing the surface-modified 17–4 PH SSFs with different matrix-based Ag NPs using traditional and digital image-based methods. In this novel study, Ag NPs prepared with Mac and Mat plant species were coated on the metallic surface and compared. Digital image-based methods, including artificial intelligence (AI)-supported SEM and color intensity processing based on RGB analysis of surface-modified 17–4 PH SSF, were used for the first time to characterize the porous structure. The significance of these characterization studies for facial or maxillofacial surgery and dental implant applications with porous materials is discussed in detail in the next part of this study.

2. Material and Method

2.1 Materials

The substrate material chosen for this research was 17–4 PH SSF, which has approximately 70% porosity and an irregular pore shape. These steel foams were manufactured by the space holder-water leaching technique in powder metallurgy. The chemical composition of the gas atomized spherical 17–4 PH stainless steel powders, which were obtained from Carpenter Powder Products in Sweden, included 4.6 wt.% Ni, 15.2 wt.% Cr, 0.7 wt.% Mo, 0.4 wt.% Nb, 4.9 wt.% Cu, 1.4 wt.% Si, and balance-Fe. The foam specimens were sintered at 1260 °C for 40 min in a Lenton UK model tube furnace under high purity hydrogen. Cylindrical specimens with a diameter of 18 mm and a height of approximately 15 mm were produced. The compressive yield strength and Young's modulus of 17–4 PH SSF compact parts produced were 49 MPa and 0.51 GPa, respectively. Details of the steel foams and fabrication processes were described in a previous paper (Ref 16). Figure 1 shows the photograph of the sintered 17–4 PH SSF.

Various materials have been used to synthesize different plant extract matrix-based Ags used to modify the surface of 17–4 PH SSF. Maca root, matcha tea, and locust bean gum in powdered form were purchased from Arifoğlu Company (Turkey). Sodium hydroxide (NaOH) was purchased from Merck Company (Germany). The filter paper (Whatman® qualitative paper, diameter: 25 mm) and silver nitrate ($AgNO_3$, purity: ≥ 99.0%) were purchased from Sigma-Aldrich Company (Germany). All chemicals and reagents were used without further purification.

2.2 Synthesis of Different Matrix-Based Ag NPs

Information on the synthesis of various plant extract matrix-based Ag NPs used in this study is provided in this section. Details on the sonochemical synthesis of Ag NPs-based nanocomposites were described in our previous papers (Ref 37, 47, 48).

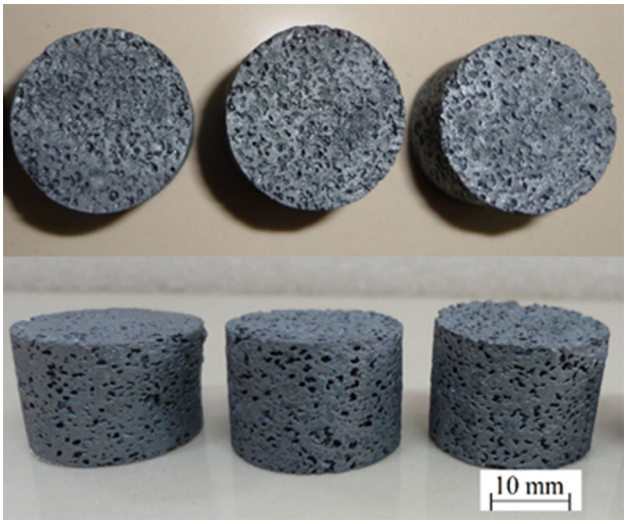

Fig. 1 Images from the top and side of the 17–4 PH SSF

2.2.1 Synthesis of Ag NPs. Ag NPs were synthesized using Mat, Mac, and Loc. For the Mat and Mac powders, 1.0 g was added to 250 mL of distilled water, stirred for 5 min, and left in the dark for 5 days at 25 °C. Then, 0.2 g of NaOH was added to 125 mL of distilled water and stirred for 10 min at room temperature. In a separate container, 0.42 g of $AgNO_3$ was dissolved in 250 mL of distilled water. Then, 1 mL of NaOH solution and 100 mL of $AgNO_3$ solution were slowly added to 50 mL of the Mat or Mac extract solution and mixed. The solution was sonicated for 30 min at an amplitude frequency of 30% at room temperature and filtered through a 0.22 μm pore size syringe filter. The Loc powder (1.0 g) was mixed with 250 mL of distilled water for 5 min and left in the dark for 5 days at 25 °C. 0.84 g of $AgNO_3$ was added to 500 mL of distilled water and mixed at room temperature. The silver solution was slowly added to the locust solution and stirred for 10 min at 25 °C. Then, 0.1 g of NaOH was dissolved in 250 mL of distilled water and slowly added to the Loc-$AgNO_3$ solution at room temperature. The solution was sonicated for 10 min at a 45% amplitude frequency at room temperature and filtered through a sterile syringe filter. The Ag NPs solutions were stored in a sterile container at room temperature in a vacuum desiccator until further use.

2.2.2 Optimization of Ag NPs. NPs composed of plant extracts can be enhanced in several ways to improve their characteristics and decrease their toxicological effects. These are a few techniques for optimizing plant extract-based NPs:

- Type of plant extract: The size, shape, and morphology of the resultant NPs can be affected by the type of plant extract because different plant extracts contain various bioactive chemicals. As a result, selecting the best plant extract can help to maximize the NPs' qualities. In this study, extracts of Mat, Mac, and Loc were utilized frequently to create NPs.
- Concentration of plant extract: The surface property of the NPs can all be significantly influenced by the concentration of plant extract employed during the synthesis process. To achieve the necessary qualities, the optimum concentration of the plant extract was established for each unique synthesis procedure. Different plant extracts (Mat, Mac, and Loc) of 4 g L−1 concentration were used for the biosynthesis of Ag NPs.
- pH and temperature: The reaction mixture's pH and temperature can have an effect on the final NPs' size and other features. As a result, changing the reaction mixture's pH and temperature can help the NPs' characteristics. Different nanostructures were produced when all samples were at 25 °C and pH 7.4.
- Stabilizing agents: Surfactants and polymers are examples of stabilizing agents that can be used to increase the stability and biocompatibility of NPs. To avoid agglomeration and enhance the NPs' dispersibility, such compounds can be added to the reaction mixture throughout the synthesis process. In this study, PEG was also used as a stabilizer to protect Ag NPs.
- Characterization: It is crucial to thoroughly evaluate plant extract-based NPs using methods including SEM, TEM, XRD, and FTIR to improve their characteristics. To ensure that nanoparticles (NPs) meet the required specifications, it is important to determine their size, shape, and composition. In this particular study, the surface properties of Mac-Ag NPs, Mat-Ag NPs, and Loc-Ag NPs were analyzed using SEM and AI-supported SEM techniques. Moreover, the particle size and surface properties of the Ag NPs were determined using TEM. XRD was performed to evaluate the crystalline structure of Ag NPs. Overall, selecting the plant extract carefully, controlling the reaction conditions, utilizing stabilizing agents, and thorough characterization are all necessary to optimize plant extract-based NPs. Plant extract-based NPs can have their qualities optimized, which will increase their biocompatibility, lessen their toxicological effects, and expand their range of potential applications.

2.3 Coating of 17–4 PH SSF with Different Matrix-Based Ag NPs

Three different matrix-based Ag NPs solutions were deposited onto 17–4 PH SSF substrates, which contained approximately 70% porosity, using drop-casting method. The process was carried out at the room temperature with a short contact time. Specifically, 8 drops (3 mL) were dispensed onto each substrate using a pasteur pipette. Then, the samples were allowed to dry at room temperature for 24 h. A schematic view of the experimental process is given in Fig. 2.

2.4 Characterization Methods

The morphology of the synthesized Ag NPs using three different matrixes was examined using a Zeiss-Sigma 300 scanning electron microscope (SEM). The surface characteristics and particle size distributions of the Ag NPs were determined by a transmission electron microscope (TEM) (Hitachi High Tech HT7700) in a high vacuum mode at 100 kV. The optical properties of the Ag NPs solutions were measured using a double-beam UV–Vis spectrophotometer (T + 80 model, PG Instrument) with an UVWin 5 Software. The crystallinity of the Ag NPs was measured by x-ray diffraction (XRD) (Rigaku D/Max2200/PC) with Cu-Kα radiation from 10° to 70° at 40 kV and 15 mA.

The pore morphology of the highly porous stainless steel specimens coated with three different types of Ag NPs was

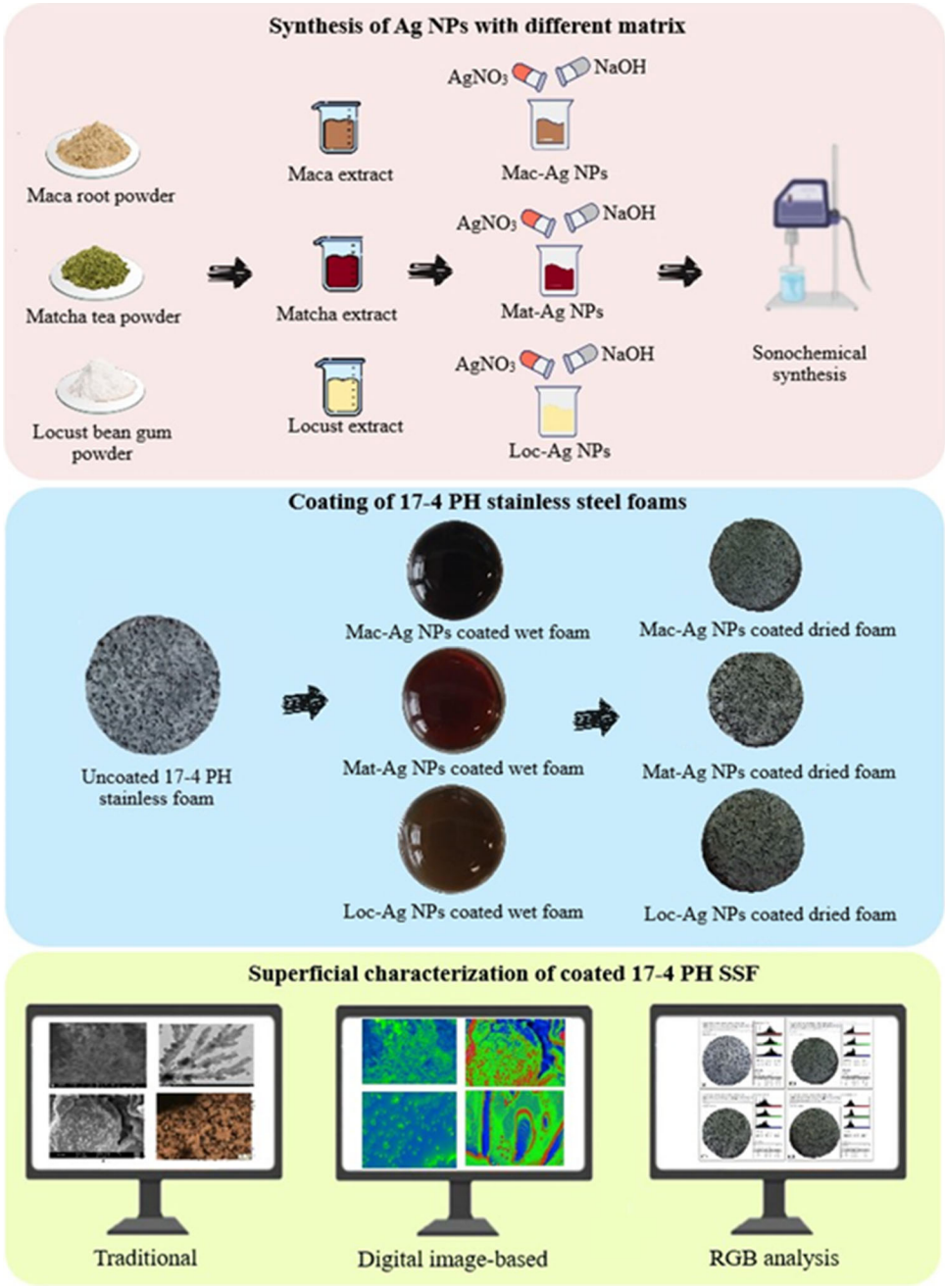

Fig. 2 Experimental steps of the processes

examined by SEM–EDS. The cross-sectional view of the coating was examined using optical microscopy (Nikon MA100). The specimens' pores were filled with a cold-hardening epoxy resin (Epofix, supplied by Struers) then etched for optical examination. The total porosity content of 17–4 PH SSF was determined using the Archimedes' principle. Measurements were performed on a Sartorius precision balance equipped with a density determination kit. To determine the open and closed porosity ratios of the coated steel foams, the samples were dipped in paraffin boiling at 150 °C. The ratios were determined by weight measurements before and after immersion. The pore size, pore size distribution, and pore shape were determined by quantitative image analysis using commercial image analyzer software (Clemex Vision PE). The area of each pore on the SEM image was calculated, and the spherical diameter was taken as pore size and sphericity as pore shape. The surface roughness values of the uncoated and coated 17–4 PH SSF specimens were measured using a SJ-201P model Mitutoyo surface roughness measurement device.

RGB analysis of the digital images was carried out using a smartphone as a simple and low-cost method of measurement with easy operation. For this purpose, photographs of all samples were taken with a smartphone camera (48 MP) under an 8 W compact fluorescent bulb. All pictures were taken from the same position. ImageJ software (1.51q) was used to obtain the colorimetric histograms of all the samples. RGB calibration was performed using black and white patterns corresponding to the color scales (255, 255, 255) and (0, 0, 0), respectively. Each

RGB primary color was represented by a vector, based on linear calibration of each color (red, green, and blue) (Ref 49). The opacity values of the coatings were calculated with using the RGB results and Eq 1 (Ref 50).

$$target = opacity.\ overlay + (1 - opacity).\ background \quad \text{(Eq 1)}$$

where, target: value of the coated surface, overlay: value of the coating solution, background: value of the uncoated 17–4 PH SSF, and opacity: value of the quality of lacking transparency or translucence of the coating on the surface.

3. Results and Discussions

3.1 Characterization of the Synthesized Different Matrix-Based Ag NPs

The properties and applications of Ag NPs are significantly influenced by their size. NPs with a size below 100 nm are believed to possess unique physical, chemical, and biological properties due to their high surface area to volume ratio. However, it is important to note that larger particles cannot be classified under this particle size range, as they may exhibit different characteristics. For example, larger particles with varying surface areas, sizes, and shapes may have different chemical interactions with other materials and living cells. Therefore, it is crucial to carefully consider the particle size range of NPs when conducting experiments and analyzing results. To ensure accurate size calculations of Ag NPs, we utilized various techniques such as SEM, AI-supported SEM, TEM, and AI-supported TEM. Electron microscopy analysis is one of the most advanced techniques for determining the micro/nanostructural, chemical, and surface properties of samples by providing image data. However, obtaining high-quality and high-resolution microscopic images can be difficult. Therefore, a simple and low-cost AI-supported imaging process was used to improve the quality of images in this study. The surface properties of Mac-Ag NPs, Mat-Ag NPs, and Loc-Ag NPs were analyzed using SEM and AI-supported SEM techniques. The SEM and AI-supported SEM images of (a) Mac-Ag NPs, (b) Mat-Ag NPs, and (c) Loc-Ag NPs are given in Fig. 3. The AI-supported SEM technique was used to understand the surface properties of the nanoformulations and to fix blurry images, which could effectively exhibit the dispersion of the Ag NPs in the matrix by ImageJ software with the Green-Fire Blue mode (8 bits). As seen in the AI-supported SEM results, it was clear that the Mac-Ag NPs, Mat-Ag NPs, and Loc-Ag NPs had spherical-like shapes with green modified colored particles, with particle diameters mostly below 50 nm with green modified colored particles. The distribution, sphericity, and regions of Ag NPs in the matrix are more clearly visible on AI-supported images. Several studies in the literature emphasize that AI-based image methods for complex small-sized nanosystems can improve high-resolution microscopic techniques, resulting in high-quality and uniform particle dispersion screening in applications (Ref 51-54).

The particle size and surface properties of the prepared Ag NPs were analyzed using TEM. The morphology results and particle size distribution histograms of a) Mac-Ag NPs, b) Mat-Ag NPs, and c) Loc-Ag NPs are presented in Fig. 4. According to the TEM results, different matrixes can exhibit widely varying properties such as dispersion, shape, and particle sizes. It is clear that Mac-Ag NPs, which have a spherical shape, Mat-Ag NPs, which have a dendrimer shape, and Loc-Ag NPs, which also have a spherical shape, all have a homogeneous nanomaterial dispersion with particle sizes of approximately 46.9, 24.7, and 47.3 nm, respectively. In this study, it was critical to investigate and understand the fundamental knowledge of the effects of bio-based matrixes on the shape and structure of nanostructures. It has been observed that the homogeneous nanomaterial dispersion and nanoparticle morphology in the matrix played a role in the origin of the particle size effect that improves the surface properties. When compared with the particle size histograms of Mac-Ag NPs, Mat-Ag NPs, and Loc-Ag NPs, we observed that all Ag NPs had relatively similar particle sizes due to electronegativity and repulsion force between NPs. However, the shape changed from spherical to dendrimer, depending on the matrix.

To determine the crystalline structure of Ag NPs in nanobiocomposite structure, XRD analysis of Mac-Ag NPs, Mat-Ag NPs, and Loc-Ag NPs was performed. The XRD pattern of nanobiocomposites is given in Fig. 5. As shown in Fig. 5, the characteristic peaks of nanobiocomposites were formed at the same points (2θ = 21.30°, 38.60°, 44.40°, and 65.60°). These peaks corresponded to JCPDS file No.00-004-0783. The peaks observed at 38.60°, 44.40°, and 65.60° corresponded to the planes of (1 1 1), (2 0 0), (2 2 0), and (3 1 1), respectively (Ref 55-58). Based on this, it can be concluded that silver crystals have a face-centered cubic structure (Ref 55, 56, 58). In addition to the stated peaks, the peak observed at 21.30° was due to the bioorganic phase of the nanobiocomposite (Ref 43).

The UV–Vis measurements of the Mac-Ag NPs, Mat-Ag NPs, and Loc-Ag NPs were performed to obtain the wavelength and absorbance spectrum. Figure 6 shows the UV–Vis spectra of nanobiocomposites with different matrixes. As seen in the graph, all nanobiostructures of Ag NPs exhibited a characteristic spectrum. It is known that synthesized Ag NPs from different extracts show characteristic peaks between 400 and 460 nm due to surface plasmon-resonance (SPR) behavior (Ref 59). Thus, characteristic Ag NPs formation is observed in all matrix structures.

3.2 Surface Characterization of Ag NPs-Coated 17–4 PH SSFs

Since the structures with high porosity have an open pore structure, the coating solution passed through the pores and went down to the bottom of the specimens. The open pore structure is due to the fact that the pores are connected to each other. Observations made in the study showed that the passage of coating solutions through the sample surface was different. Mac-Ag NPs solution rapidly flowed through the pores of the foam, accumulating at the bottom of the sample. The Mat-Ag NPs solution remained on the sample surface and flowed very slowly through the pores. Loc-Ag NPs solution, on the other hand, was absorbed very quickly by the sample surface and very little went to the bottom, similar to a sponge absorbing water. The color of all coated steel foams changed significantly after drying based on the plant extract solution used for the coating. The most important factors that affect the contact angle are the surface energy and surface roughness of the solid. As the surface roughness increases, both the hydrophilic and hydrophobic properties also increase. The 17–4 PH SSFs used

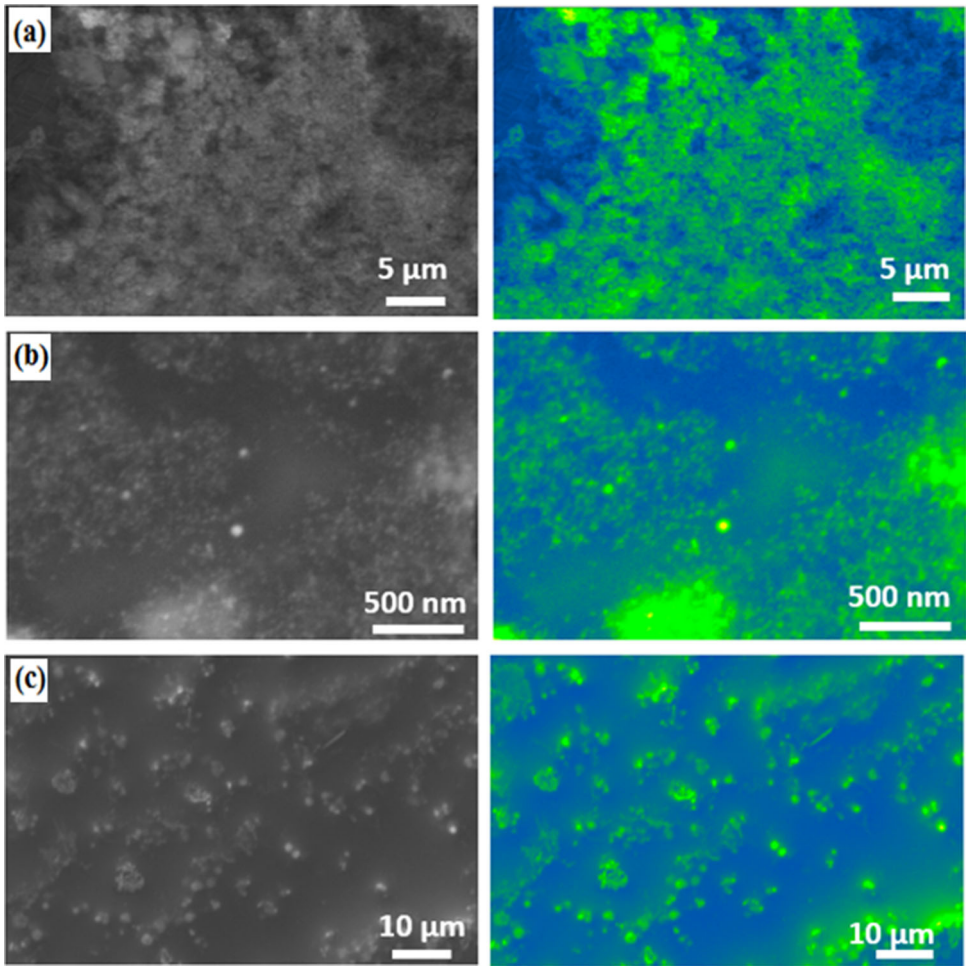

Fig. 3 The SEM (left) and AI-supported SEM images (right) of (a) Mac-Ag NPs, (b) Mat-Ag NPs, and (c) Loc-Ag NPs

in the study exhibit high surface roughness due to their macropore structure and production method. Unlike ideal surfaces, the formation of a composite interface (CI) occurs for solid surfaces with high surface roughness (Ref 60). The different viscosities and surface tensions of the solutions affect their passage through the porous structure and the rate of transition. This difference also affects the cohesion and adhesion forces (Ref 61). In the coating with Mat-Ag NPs, it is thought that the coating solution cannot fully wet the surface and remains on the surface due to greater cohesion force than the adhesion force. In contrast, in the coating with Mac-Ag NPs and Loc-Ag NPs, the opposite situation occurred, and wetting was almost complete. This is assumed to be due to the adhesion force being lower than the cohesion force. Many studies on surface tension have discussed the effects of this relationship between forces on wetting or non-wetting (Ref 62-64). In the spreading wetting observed in the coating of all samples, the liquid tries to increase the liquid, solid–liquid, and gas–liquid interface in contact with the solid and to reduce the solid–gas interface (Ref 60).

The SEM and AI-supported SEM images of the different matrix-based Ag NPs-coated 17–4 PH SSF surfaces are given in Fig. 7**.** The AI-supported SEM images of Mac-Ag NPs, Mat-Ag NPs, and Loc-Ag NPs-coated 17–4 PH SSFs were able to remove noise from images using an averaging filter in 8-bit/rainbow RGB mode while enhancing the image quality of samples. The 17–4 PH SSFs have a relatively uniform pore distribution, and the cell walls separating each macropore from the other macropore are clearly visible. The morphology of the final pores has an irregular structure, and no cracks were observed in the pore walls of the highly porous structures. A large number of micropores were observed in the cell walls due to the production method of the 17–4 PH SSFs, which involves incomplete sintering of the steel powder (Ref 65). These features are valid for all coated steel foams. At larger magnifications, the original structure of the coating material is fully visible and it can be seen that the Ag NPs are homogeneously dispersed on the substrate surface. The homogeneous distribution of Ag NPs on the substrate increases the resistance properties. Jothi et al. coated the surface of stainless steel with Ag NPs and found that the homogeneous distribution of nanoparticles increases the resistance properties of the substrate (Ref 66). The near-spherical shape of the Ag NPs is evident in all coatings. Distribution of Ag NPs, while it is more distant on the surfaces coated with Mac-Ag NPs and Loc-Ag NPs, a denser distribution is observed on the surfaces coated with Mat-Ag NPs. The distribution and shape of NPs on the substrate are consistent with the studies on metallic surfaces coated with Ag NPs (Ref 67-69). Velasco et al. reported that the mobility of Ag NPs is quite versatile and continues in the direction of movement of agglomerated Ag NPs on the coated surface (Ref 68). According to the results from AI-supported

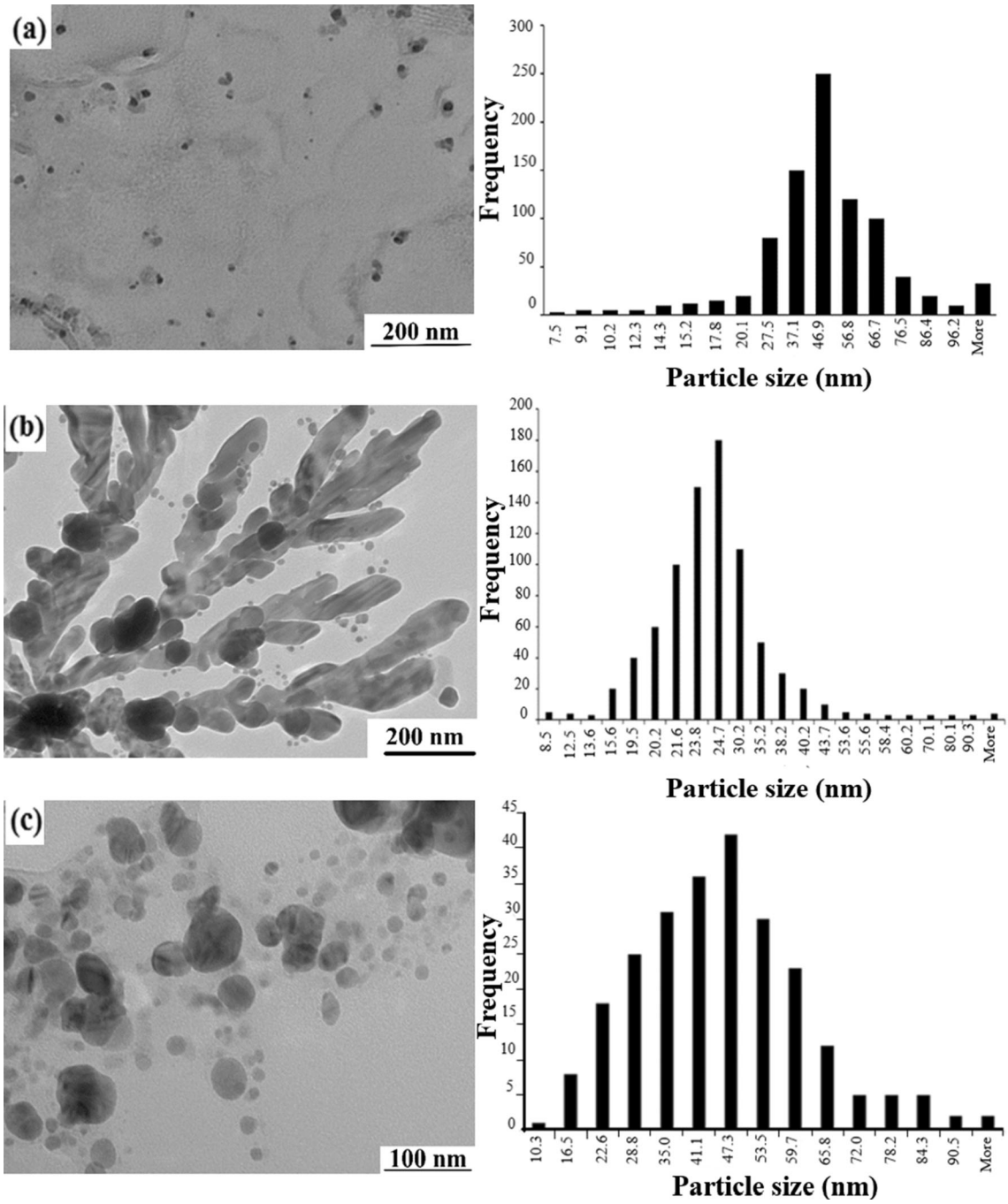

Fig. 4 TEM images (left) and particle size distribution histograms (right) of a) Mac-Ag NPs, b) Mat-Ag NPs, and c) Loc-Ag NPs

SEM, Ag NPs on the surface coated with Mac-Ag NPs had a spherical-like shape with green modified colored particles and are concentrated in the interior of the pore walls. Ag NPs on the steel foam surface coated with Mat-Ag NPs were well dispersed and had spherical-like shapes with red modified colored particles. Ag NPs on the surface coated with Loc-Ag NPs were concentrated around the macropores and had spherical-like shapes with green modified colored particles.

EDS analysis results obtained from SEM images are shown in Fig. 8. The presence of Ag is attributed to the formation of Ag NPs, while the presence of Na atoms is believed to be due to the plant extract, and the presence of O is thought to result from the oxidation of Ag ions. Fe, Cr, and Ni atoms observed in the coated surface are from the elemental signatures of the stainless steel substrate material. Similar approaches have been mentioned in the study conducted by Şahin on the synthesis and characterization of Ag NPs (Ref 70).

3.3 Structural Characteristics of Pores in the Ag NPs-Coated 17–4 PH SSF

Usually, metallic foams are structurally characterized by pore size, shape, sphericity, distribution, pore topology (open and closed pores), and porosity content (Ref 71). Mutlu and Oktay produced highly porous 17–4 PH SSF for biomedical applications and stated that the porosity, pore shape, and size

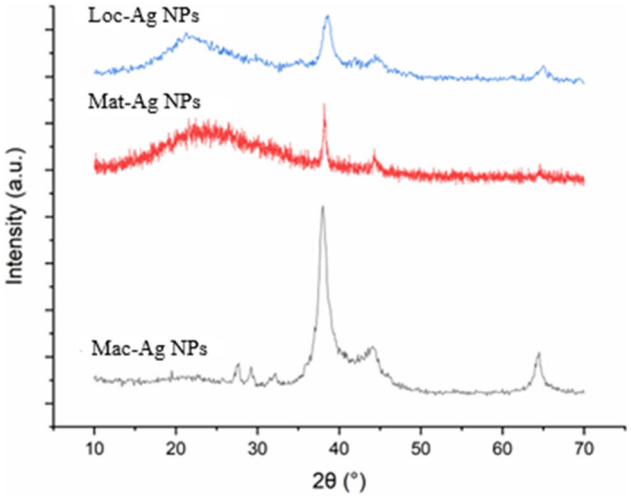

Fig. 5 XRD pattern of the synthesized different matrix-based Ag NPs

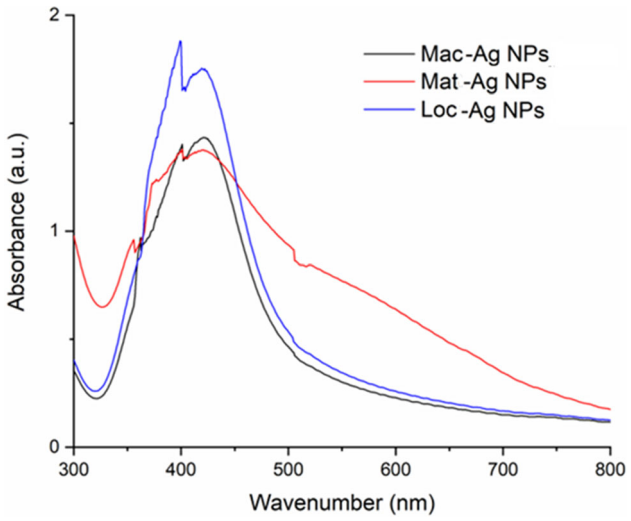

Fig. 6 UV–Vis spectra of the synthesized different matrix-based Ag NPs

play an important role in bone ingrowth (Ref 72). The material surface of implants is susceptible to external influences such as corrosion, oxidation, wear, and fatigue, which lead to various material deteriorations that start at the surface. Costly and complex operations are performed every year to revise failed implants. Therefore, it is essential to characterize the coated surface to better understand the effects of coating with different nanocomposites on the structural characteristics of the porous structure. The selection of metal foams depends on their morphology (content, size, shape, and sphericity of the pores) and their mechanical properties (Ref 73). In this study, all superficial properties were determined for uncoated and coated SSFs with different matrix-based Ag NPs. The image analyzer software on the SEM images was used to determine the macro and micro pore size and the sphericity of the SSFs. Table 1 presents the porosity content, value ranges of microporosity in pore wall, macro pore size, pore shape, and mean pore sphericity of the SSFs coated by different matrix-based Ag NPs and also SSF for comparison. To the best of our knowledge, these properties have not been investigated in studies on the coating of metallic foam structures. Therefore, a detailed study on the impact of Ag NPs on the coating is required.

The SEM images presented in Fig. 7 reveal that SSFs are composed of two types of pores: macropores and micropores in their cell walls. Although macropores may appear to be isolated from each other, they are actually connected to each other through micropores in the cell walls. Therefore, the presence of macro and micro pores directly affects the interconnectivity feature. Uncoated foams exhibit a 13.59% microporosity ratio in the pore wall, an 879.6 μm macro pore size, and a 0.59 pore sphericity, while the coated foams have microporosity ratios ranging from 12.25 to 12.78% in the pore wall, macro pore sizes ranging from 789.5 to 887.4 μm, and pore sphericity values ranging from 0.58 to 0.59. The macro pore size, pore shape, and sphericity values did not significantly change after coating with Ag NPs coatings, while the microporosity ratio in the pore wall decreased between 5.9 and 9.8% in all coatings. This can be explained by the penetration of the coating solution into the micropores and settling there. The presence of microporosity in the pore wall regions in the foam structure has a significant impact on the mechanical characteristics of the steel foams (Ref 2, 74). The decreases in the microporosity ratio in the coatings made with this study may cause improvement in mechanical properties. This is very important in terms of improving the properties of the porous structure. The microporosity could be partly eliminated by different matrix-based Ag NPs coating on the surface of the porous structure. However, the microporosity formed in foam structures is very important for the initial formation of osseointegration in biomedical materials (Ref 75, 76). Also, Young's modulus and compressive yield strength of cancellous bone are 0.09–1.5 GPa and 40–150 MPa, respectively. When the obtained results are compared with the literature, the structural and mechanical properties of 17–4 PH SSF are very close to those of cancellous bones. After coating, the determined average size and average sphericity values of the pores are suitable for biomedical applications (Ref 77-79). According to Smith et al., understanding the pore characteristics of the foam structure is important for tissue engineering to more accurately fabricate scaffolds, promote bone growth, and vascularization in the foam structure used as a biomaterial (Ref 76). The understanding of the pore characteristics of the foam structure is critical for tissue engineering to fabricate scaffolds, promote bone growth, and vascularization in the foam structure used as a biomaterial. Since the surface quality of manufactured implants is critical to their service performance, surface treatments play a vital role in improving the functional performance of metallic implants.

3.4 The Coating Thickness and Surface Roughness of Coated 17–4 PH SSFs with Ag NPs

There are many studies in the literature on the relationship between the biocompatibility of biomaterials and their surface properties. Considering the previous studies on the effects of surface properties of metallic biomaterials on their biocompatibility, it can be observed that in addition to the important effect of surface chemistry, the coating thickness and surface roughness affect the surface energy and they are crucial for the adhesion behavior of cells and that the topographical properties strongly influence the growth and spreading behavior of cells (Ref 80-82). Therefore, multifaceted studies with surface modifications of biomaterials to be used as implants are

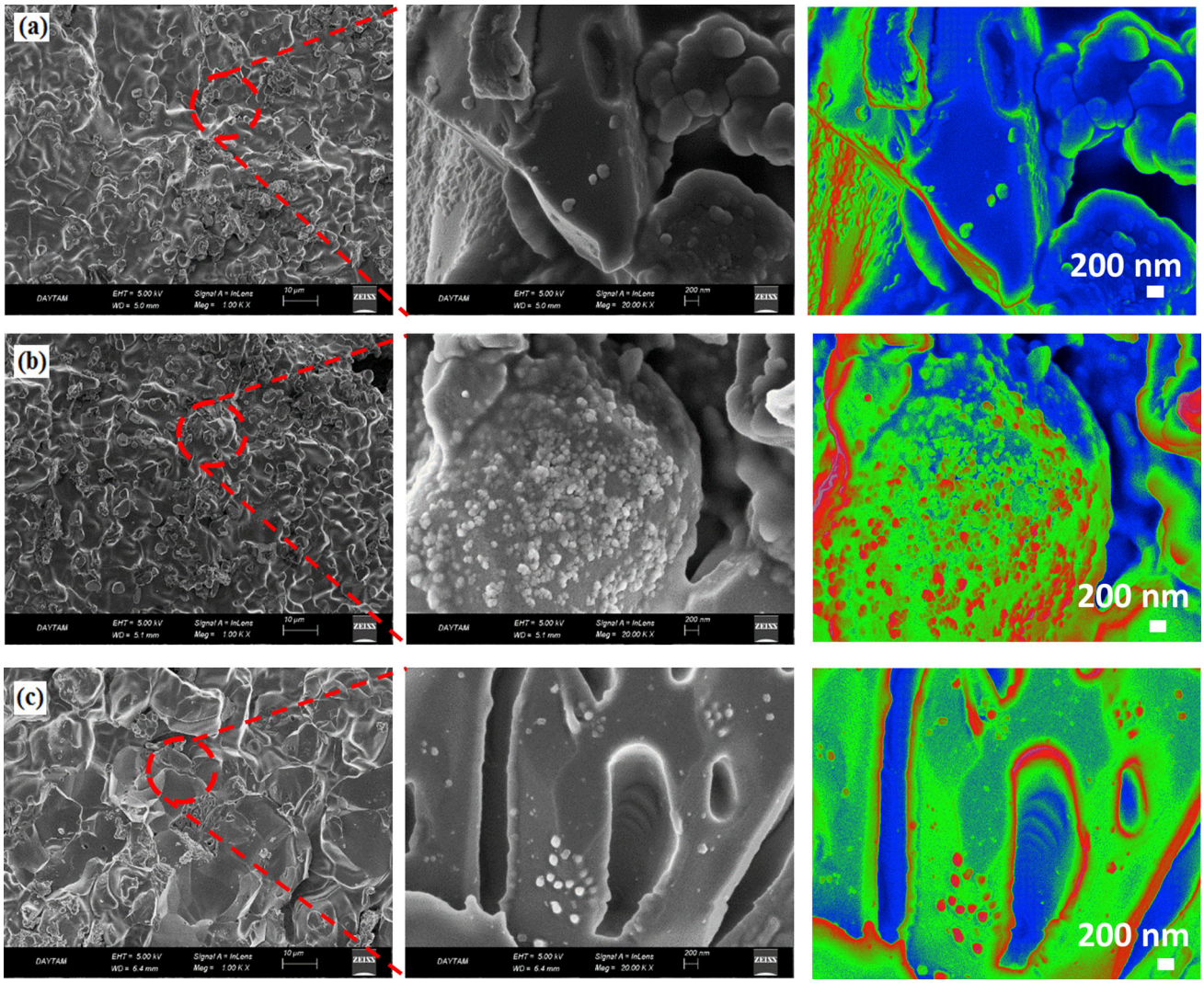

Fig. 7 The SEM (100kx-left and 20.00kx-middle) and AI-supported SEM (right) images of the different matrix-based Ag NPs-coated 17–4 PH SSFs: (a) Mac-Ag NPs, (b) Mat-Ag NPs, and (c) Loc-Ag NPs

important. The presence of micropores in the pore walls surrounding the macropores due to the production method of the foamy structure is a desirable feature for vascularization in biomedical (Ref 83, 84).

Table 2 presents the surface roughness, coating thickness, and change in weight of the different matrix-based Ag NPs coated on 17–4 PH SSFs. The interface coating thickness values of Mac-Ag NPs, Mat-Ag NPs, and Loc-Ag NPs-coated steel foams were measured using an optical microscope in the ranges of 5.4-7.3, 5.8-7.5, and 5.7-6.8 μm, respectively. It is seen that the coatings exhibit continuity in the side section surface morphology examinations. The average coating thickness of the steel foams coated with different matrix-based Ag NPs is between 6.2 and 6.6 μm, very close to each other. The image analyzes have shown that Ag NPs were coated in a single-layer and homogeneously on the steel foam structure in all coatings. Alias et al. defined the structure on the surface as a monolayer structure (Ref 84). The surface roughness value of materials affects many properties, such as abrasion, chemical stability, and microhardness (Ref 66). Therefore, it is important to know the changes in surface roughness properties after coating. The average surface roughness values of uncoated 17–4 PH SSF surfaces are approximately 4.58 μm. For 17–4 PH SSF surfaces coated with Mac-Ag NPs, Mat-Ag NPs, and Loc-Ag NPs, surface roughness values were measured in the ranges of 4.98-5.11 μm, 5.01-5.67 μm, and 5.06-5.18 μm, respectively. Surface roughness values after coating, Mac-Ag NPs, Mat-Ag NPs, and Loc-Ag NPs-coated steel foams increased by 10, 11, and 11%, respectively. This can be explained by the distribution of the coating solutions on the surface of the highly porous substrate. The coating solutions have flowed into the steel foam due to the open pore structure of the steel foam. From the images, it can be seen that it has penetrated into the micropores. Başargan (Ref 85) investigated the morphology of the coated surfaces with Ag, and found an increase in surface roughness due to the continuity of the coating. In Table 2, the change in coating weights is given as an increase. Similar weight changes were measured in all three nanocomposite coatings. According to the test results, the changes in coating thickness, surface roughness, and weight values were determined in all Ag NPs coatings. Surface roughness and coating thickness are important features for the structural and functional areas of using the materials. In this

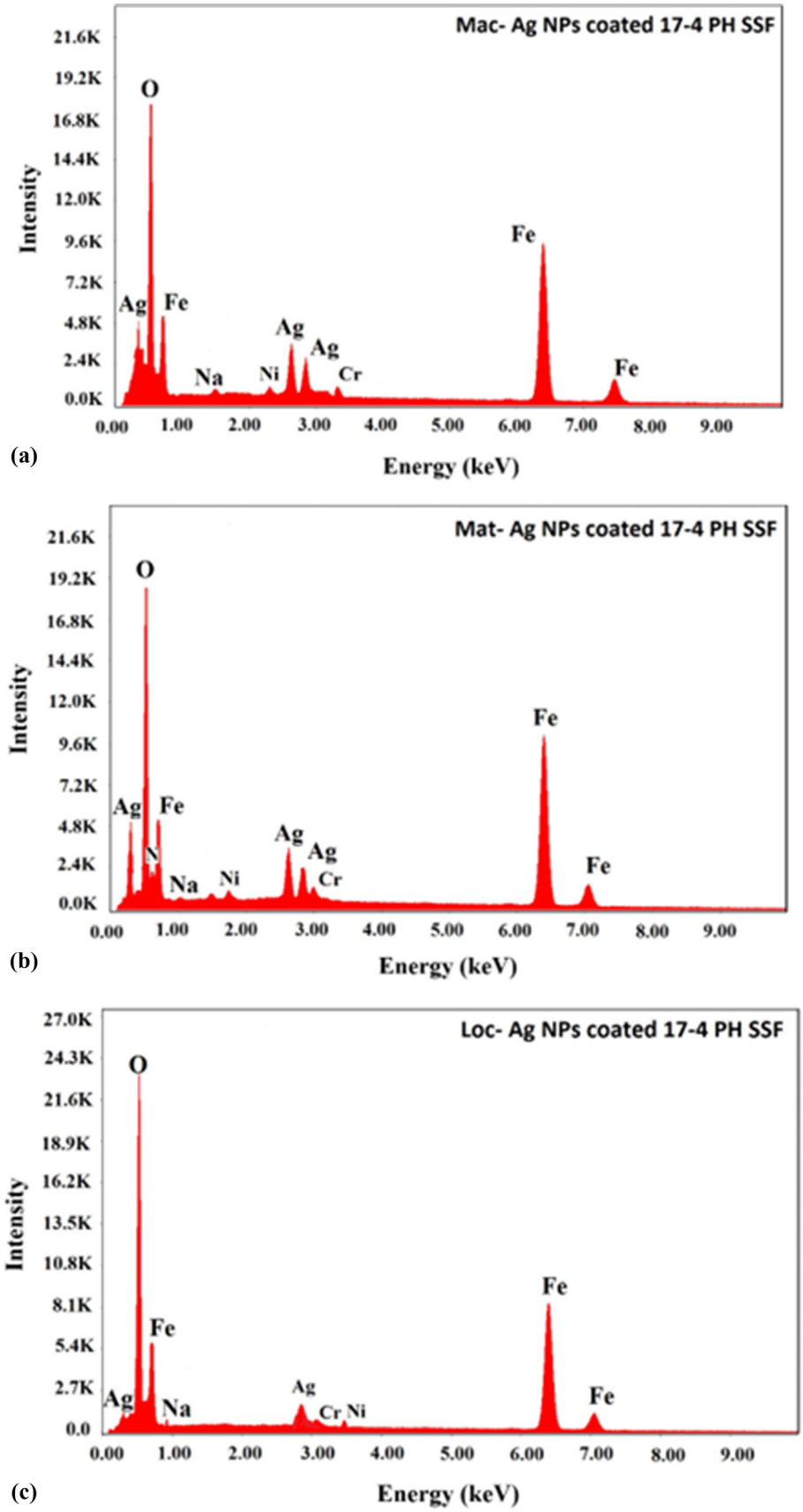

Fig. 8 EDS analyzes of the different matrix-based Ag NPs-coated 17–4 PH SSFs: (a) Mac-Ag NPs, (b) Mat-Ag NPs, and (c) Loc-Ag NPs

Table 1 The porosity, microporosity in pore wall, macro pore size, and pore sphericity of the 17–4 PH SSFs

Materials	Porosity, %	Micropore ratio in pore wall, %	Macro pore size, μm	Pore sphericity
Uncoated foam	70.4 ± 1.8	13.59 ± 0.41	879.6 ± 113	0.59 ± 0,19
Mat-Ag NPs-coated foam	70.8 ± 1.3	12.78 ± 0.35	887.4 ± 92	0.58 ± 0,21
Mac-Ag NPs-coated foam	70.1 ± 1.2	12.25 ± 0.29	789.5 ± 122	0.59 ± 0,18
Loc-Ag NPs-coated foam	71.2 ± 1.5	12.47 ± 0.33	859.6 ± 118	0.59 ± 0,20

Table 2 The coating thickness, surface roughness, and change in weight of the Ag NPs-coated 17–4 PH SSFs

Material	Coating thickness, μm	Surface roughness, Ra, μm	Change in weight, %
Mac-Ag NPs-coated foam	5.4-7.3	4.98-5.11	3.21 ± 0.15
Mat-Ag NPs-coated foam	5.8-7.5	5.01-5.17	3.27 ± 0.11
Loc-Ag NPs-coated foam	5.7-6.8	5.06-5.18	3.16 ± 0.09

sense, it is important to determine these values and their changes in this study.

3.5 The RGB Analysis and Calculations of Opacity of the Ag NPs-Coated 17–4 PH SSFs

Digital image processing based on a RGB color analysis of the coated SSFs is obtained by varying the recombination probabilities taken from a particular area of the part (Ref 86). Processing the color intensity of digital images based on RGB analysis is helpful in detecting physiological changes, as color variations reflect physiological changes (Ref 87). In this study, RGB analysis and opacity calculations of uncoated and coated steel foams were performed for the first time. RGB analysis, which is very simple and inexpensive, can be used to determine color changes caused by coating solutions on the surface. Considering the application areas of metallic foams, this is an important issue for biomaterial applications. In particular, where it is used in visible locations such as dental implants, the colors of the abutment should be esthetically compatible (Ref 88, 89). In this section, a preliminary study was made for future studies.

The RGB pixels of the different matrix-based Ag NPs-coated steel foam photographs were analyzed to investigate the effect of coating materials on the surface. In Fig. 9, RGB analysis images were given of the Mac-Ag NPs (Fig. 9a), Mat-Ag NPs (Fig. 9b), and Loc-Ag NPs (Fig. 9c) in wet form on the surface of the 17–4 PH SSF. In Fig. 10, RGB analysis images were given of the uncoated (Fig. 10a) and superficially modified metal foams with Mac-Ag NPs (Fig. 10b), Mat-Ag NPs (Fig. 10c), and Loc-Ag NPs (Fig. 10d). In Fig. 11, colorimetric histogram distributions in red (Fig. 11a), green (Fig. 11b), and blue (Fig. 11c) colors obtained as a result of RGB analysis are given in Fig. 11. RGB analysis is an easy, fast, and economical method for observing and interpreting the visual change caused by the coating on the surface. RGB density results are calculated in the range of 0 (black) to 255 (white). As seen in the graphics in Fig. 11, the color values of the analysis performed on the uncoated sample and coated samples with the Loc-Ag NPs solution showed the most significant color differences. In fact, according to the figures and analyses made on the wet surfaces, it is seen that the Mac-Ag NPs solution has darker color values. In this case, it is expected that the color change after coating with Mac-Ag NPs will be close to darker values. The reason why this does not happen is interpreted as the absorption of the Mac-Ag NPs solution that was mentioned earlier from the foam surface directly into the pores. In connection with this, it is explained that the color change is greater than with other coatings due to the fact that Loc-Ag NPs stay on the surface for a while. Acevedo et al. reported that the RGB image analysis enables the physical variables to be examined according to surface color by showing the relationship between color and surface concentration (Ref 49).

Each RGB value (255, 255, 255) has the maximum value of the frequency in digital color (Ref 90). The results obtained from the RGB color analysis for all peaks are given in Table 3. The results in this study showed that the red, green, and blue values (12.68, 12.14, 13.91) were close to each other in Mac-Ag NPs solution. The red, green, and blue values of Mat-Ag NPs, and Loc-Ag NPs coating solutions were also quite different from each other. The red values in Mat-Ag NPs and Loc-Ag NPs solutions were higher than the others. The red, green, and blue values (134.73, 140.11, 148.29) of the uncoated sample are close to each other. After coating, the RGB values decreased in all samples depending on the coating solution. The green value was higher than the average value of red and blue in all coatings. Sarrafzadeh et al. stated that the results obtained from the RGB analysis of macroscopic images show a significant color change with the different concentrations of the samples (Ref 87).

To fully understand the effect of coating with different Ag NPs on the surface quality, opacity values were also calculated using RGB results. Factors such as coating thickness, surface roughness, and properties of the coated material (concentration, viscosity, type, etc.) affect the opacity quite highly. Generally, increasing coating thickness and surface roughness values increase opacity (Ref 91). It is very important to know the opacity value according to the usage area and usage conditions of the material. There are few studies on the coating of metallic foams and no studies on opacity. This study has original value in the literature in terms of the first study of the relationship metal foam surface coating with different Ag NPs and opacity. The opacity values obtained from the RGB color analysis for all peaks are given in Table 4. For steel foam surfaces coated with Mac-Ag NPs, Mat-Ag NPs, and Loc-Ag NPs, mean opacity values were calculated as 42.29, 40.26, and 41.58%, respectively. When all three coated surfaces are compared to each other, the average opacity values were very close to each other. The effect of different Ag NPs coatings on the opacity change

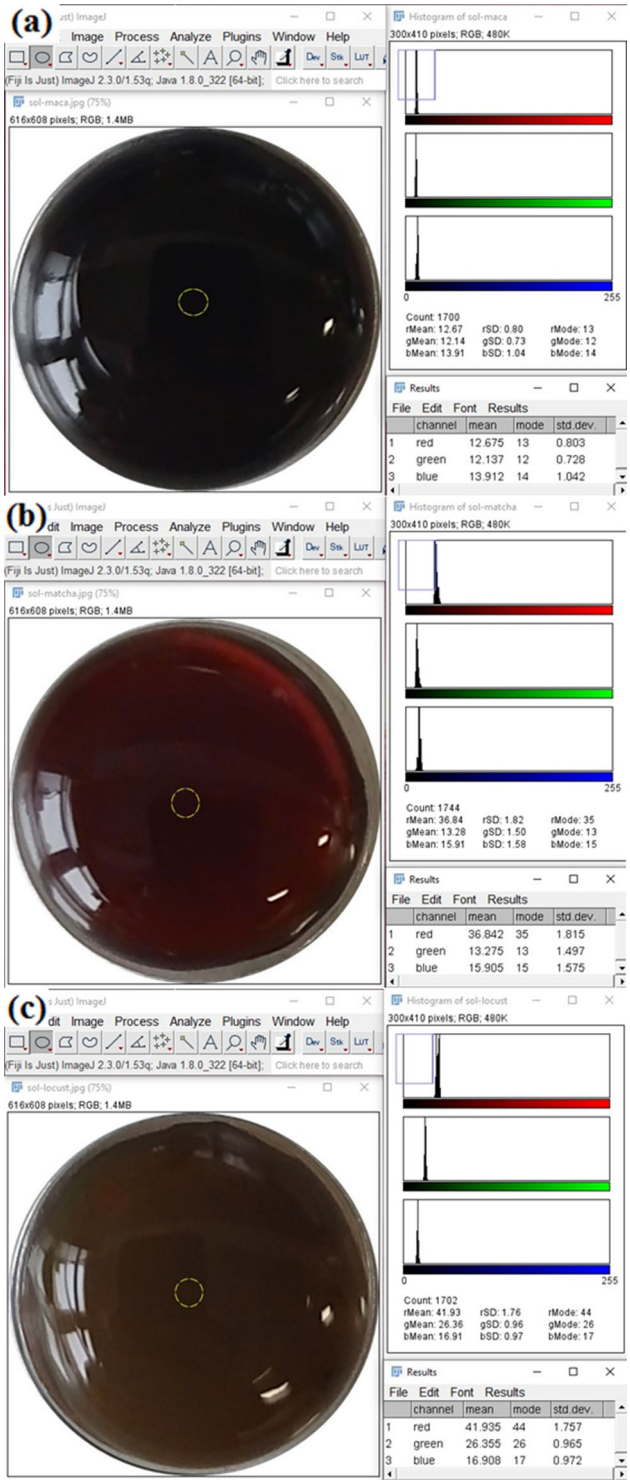

Fig. 9 RGB analysis images of the coated wet samples Ag NPs with different matrixes: (a) Mac-Ag NPs, (b) Mat-Ag NPs, and (c) Loc-Ag NPs

is not significant. This similarity can be explained by the uniform opacity created by the scattering layer across the wavelength range (Ref 92). This closeness in opacity values is also in agreement with the results of structural characterization, coating thickness, and surface roughness given in the previous sections. As a result, opacity values calculated by the RGB analysis and RGB results can be considered a simple way to visually evaluate the nanostructured coating in a cost-effective and easy way. The digital image processing in this research could have great potential as a cost-effective technique to study surface properties in various research fields.

The RGB analysis and opacity calculations of metallic foam materials to be used for biomedical applications after surface modification are important in terms of improving their functionality, including surface integrity and service performance. One of the areas where porous metallic materials are most commonly used is orthodontic implants. Each person has a gingival structure of different color and transparency, according to its own genetic structure (Ref 93). The abutment part of the implant material is visible from the outside, according to the gingival structure and creates an esthetically unpleasant appearance. The position of the dental implant placed in the jawbone and the gingival colors naturally occurring in humans are shown in Fig. 12. In this field, there are studies on the development of artificial gingival colors (Ref 93, 94). In addition, it is also possible to achieve harmony with the gingival color by providing color changes with the coating of the abutment. RGB analysis is a quick and easy method for this type of color matching and variation analysis. In this study, RGB analysis was performed to detect the small changes in the material surface after coating and to test its applicability. The calculation of opacity was also made from the values obtained after the analysis of RGB. The degree of opacity of metallic surfaces is also important in areas such as military vehicles and weapons. It has been shown that these calculations and adjustments can be realized by RGB analysis. This comparative study demonstrates the potential of RGB analysis by applying it to coated surfaces for the first time. The color variations, opacity values, and distributions of colors on surfaces can be easily detected with RGB analysis. Thanks to these results, coloration and compatibility studies can be easily performed.

3.6 Sustainable and Green Approach of this Study

Today, the concepts of sustainability and green approach, which are outputs of research and innovation activities, influence and complement each other. The concept of sustainability is an understanding that takes the necessary measures to protect the future, the consumption of natural resources, and environmental and social needs. The green approach aims to improve the quality of life and develop sustainable systems worldwide. For a process to be defined as a green process, it must be sustainable. In this sense, nanotechnology, with its impact on important issues, makes an important contribution to achieving this goal such as the proper use of energy and natural resources, attention to environmental problems and efforts to eliminate them, the prevention of waste, and the preservation of clean air and water. The role of nanotechnology in designing sustainable processes is particularly evident in nanomaterials. Nanomaterials have retained many superior properties and can be used in many fields such as health, energy, environment, manufacturing, and safety. Nanocoatings with the surface properties they offer in nanomaterials help to provide surfaces that are antibacterial, self-cleaning, protect against UV rays, and scratch and abrasion resistant. Thanks to the different properties of NPs, nanocoatings can be given different functions. The most important result in terms of sustainability is to extend the life of materials, reduce the consumption of resources and energy, and achieve positive results in terms of human and environmental health. The continuation of studies in the field of

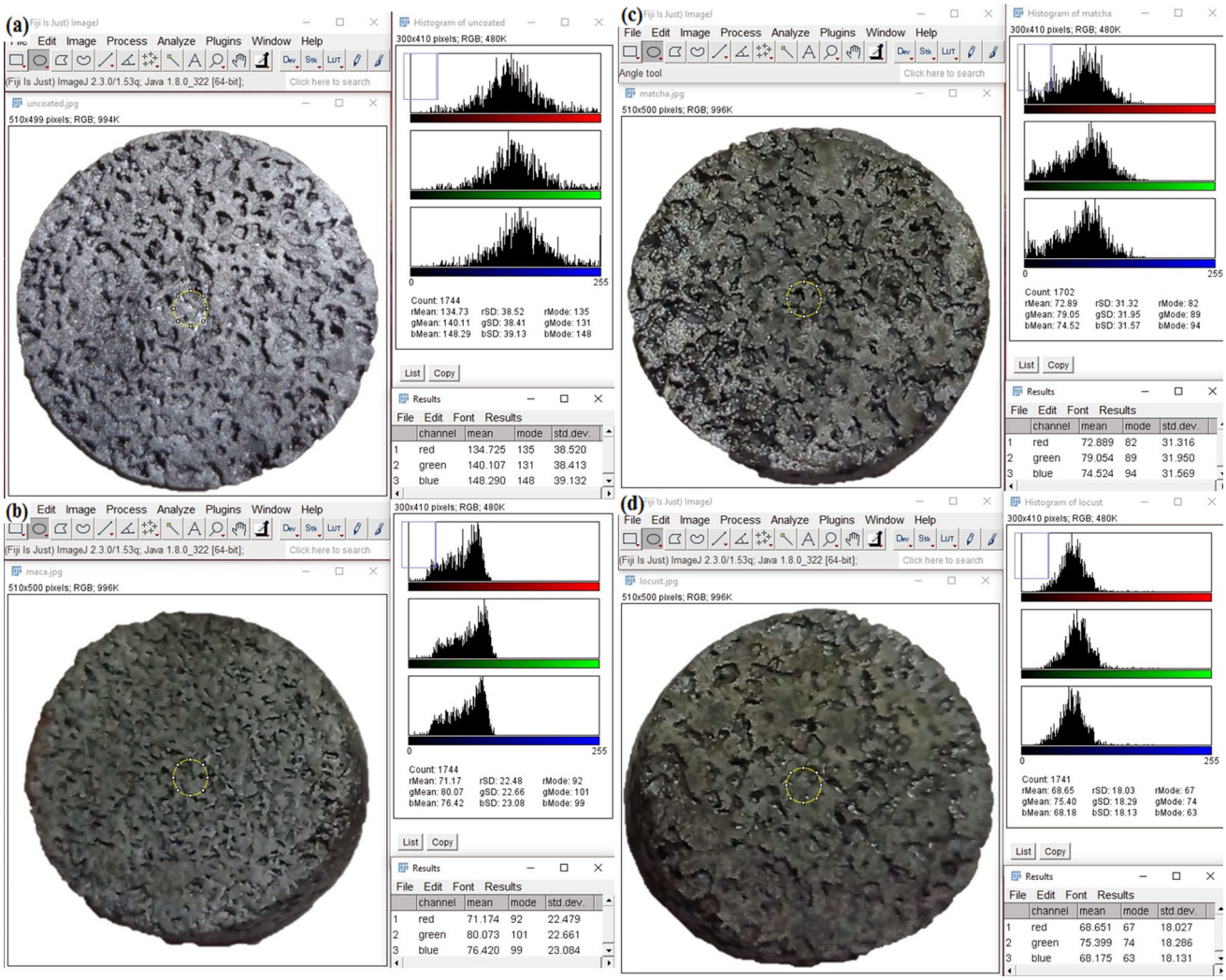

Fig. 10 RGB analysis images of the dried samples: (a) uncoated, (b) Mac-Ag NPs-coated, (c) Mat-Ag NPs-coated, and (d) Loc-Ag NPs-coated 17-PH SSFs

nanotechnology at an increasing rate, the difficulty of nanoscale fabrication and characterization, the high cost of nanomaterials, the need for specialized equipment and experience, and the development of relevant standards are barriers to the widespread application of nanotechnology. As in other technological areas, innovation is not only required in terms of the environment and human health, but potential hazards must also be identified. For the implementation of sustainability principles in the field of nanotechnology, the continuity of studies in this field and the sharing of results are very important. All processes in this study are environmentally friendly green techniques: synthesis of Ag NPs (Ref 37, 47, 48), the production method of 17–4 PH SSF with high porosity (Ref 73) used in the study, and the coating technique used in the coating of substrates (Ref 37). It covers almost all the principles of the green approach to sustainability shown in Fig. 13. A more sustainable and green approach will undoubtedly benefit our environment. All production processes and characterization results of the study are presented in detail. In terms of sustainability, it is very important that this study documents process and product information for scientific and industrial researchers working in this field.

4. Conclusions

The surface of 17–4 PH SSFs was modified with Mac-Ag NPs, Mat-Ag NPs, and Loc-Ag NPs obtained from different plant extracts and characterized by traditional and digital image-based methods to determine their superficial properties and enhance their applicability in the biomedical field. The results of the present study are as follows:

- The synthesized Ag NPs were homogeneously distributed and showed good dispersion in the maca, matcha, and locust matrixes. The synthesized Mac-Ag NPs and Loc-Ag NPs had a spherical shape with a particle diameter mostly below 50 nm. The synthesized Mat-Ag NPs have a dendrimer-like shape, with particle diameters mostly below 100 nm. All nanobiocomposites of Ag NPs showed the characteristic spectrum.
- During the coating of the highly porous surface, the coating solution penetrated through the open pores and accumulated at the bottom of the specimens. The flow of the coating solution through the pores differed depending on Ag NPs with different physical properties. This issue can

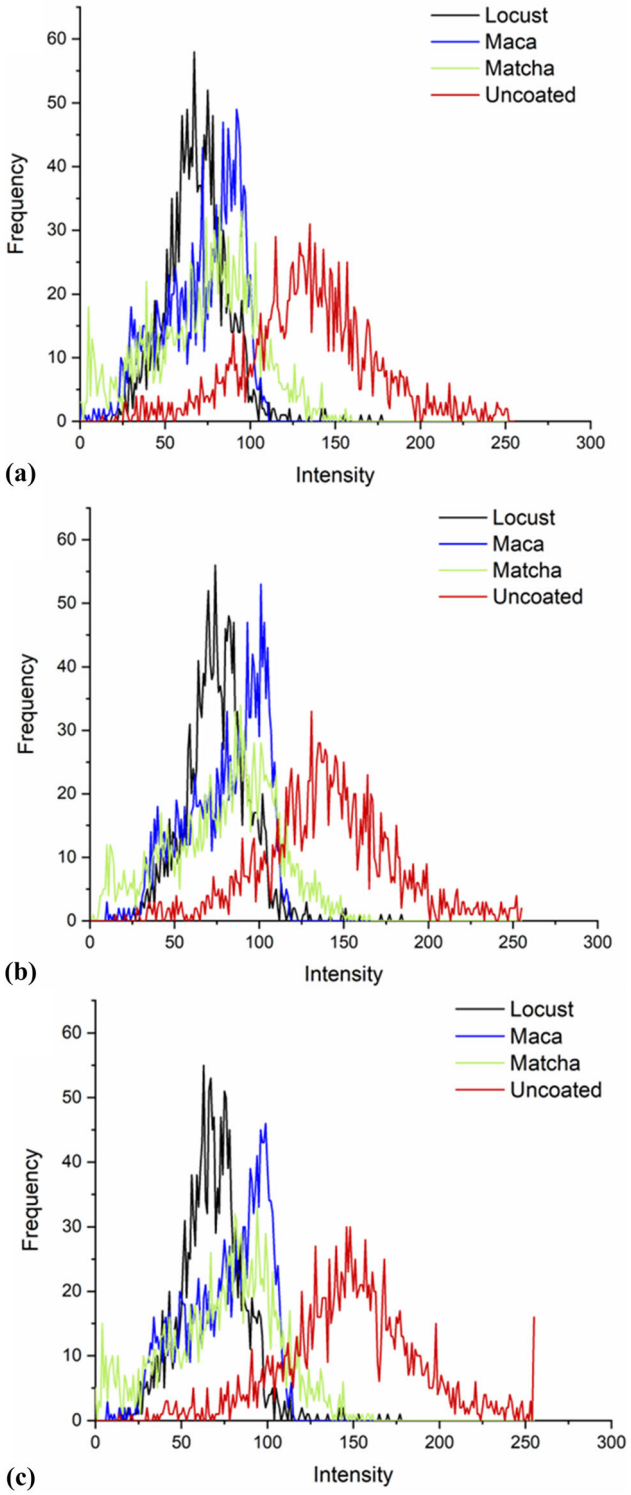

Fig. 11 The colorimetric histograms of RGB analysis: (a) red, (b) green, and (c) blue

be addressed in more detail in our future work.

- The Ag NPs on the surface of the superficially modified SSFs were more homogeneously distributed. The macropore size, pore shape, and sphericity values of the SSFs did not change significantly for the different coatings with matrix-based Ag NPs. However, the ratio of microporosity in the pore wall decreased for all coatings.

Table 3 The results obtained from the RGB analysis

RGB samples	Red	Green	Blue
Mac-Ag NPs solution	12.68	12.14	13.91
Mat-Ag NPs solution	36.84	13.28	15.91
Loc-Ag NPs solution	41.94	26.36	16.91
Uncoated 17–4 PH SSF	134.73	140.11	148.29
Mac-Ag NPs-coated foam	71.17	80.07	76.42
Mat-Ag NPs-coated foam	72.89	79.05	74.52
Loc-Ag NPs-coated foam	68.65	75.40	68.18

Table 4 The opacity values obtained from the RGB analysis

Coated samples	Opacity of red, %	Opacity of green, %	Opacity of blue, %	Mean opacity, %
Maca-Ag NPs-coated foam	43.12	39.44	44.31	42.29
Mat-Ag NPs-coated foam	36.04	39.81	44.93	40.26
Loc-Ag NPs-coated foam	37.40	38.87	48.49	41.58



Fig. 12 The gingival colors and placement of the dental implant in the jawbone

- A uniform transition layer formed between the surface of the SSF and the Ag NPs coating composed of different matrixes without cracks or delamination. Surface roughness values of all the superficially modified SSFs increased slightly.
- The results of RGB analysis and opacity values showed differences depending on the coating solution obtained from different plant extracts. These results may improve the applicability of 17–4 PH SSFs in the biomedical field, especially in dental applications.
- According to the results of this study, the superficial properties of superficially modified 17–4 PH SSFs with differ-

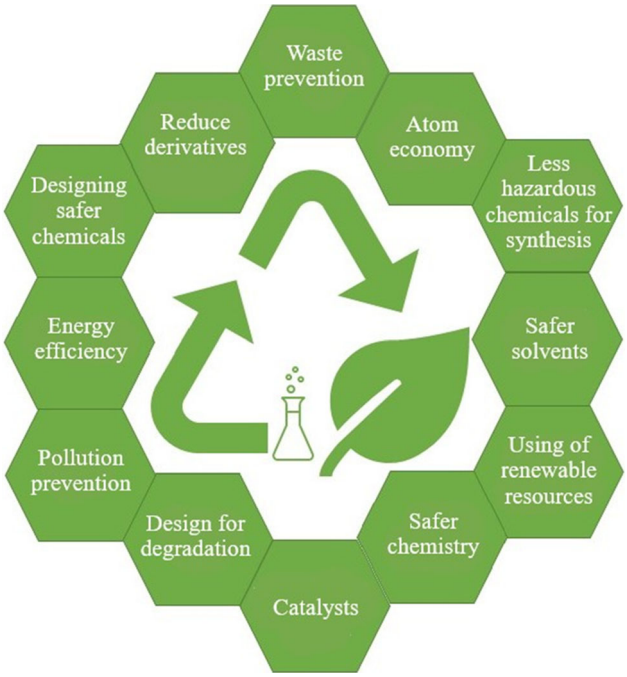

Fig. 13 The green approach principles for sustainability

ent matrix-based Ag NPs can be developed for many applications.

- Due to the cost-effectiveness and environmental friendliness of all production steps used in the study, it has significant potential to be a promising nanocoating for applications of 17–4 PH SSFs.

Acknowledgments

This study was funded by Scientific Research Projects Coordination Unit of Istanbul University-Cerrahpasa. Project Number: FYL-2019—33,913.

CRediT Authorship Contribution Statement

NBÜ was involved in writing—review & editing, supervision, project administration. GK helped in writing—review & editing, methodology, visualization. SK contributed to writing—review & editing, visualization, methodology, resources.

Data Availability

The authors confirm that experimental data and materials reported in this paper are available.

Conflict of interest

The authors declare that they have no known competing financial interests or personal relationships that could have appeared to influence the work reported in this paper.

References

1. H. Sazegaran and M. Hojati, Effects of Copper Content on Microstructure and Mechanical Properties of Open-Cell Steel Foams, *Int. J. Miner. Metall. Mater.*, 2019, **26**(5), p 588–596. https://doi.org/10.1007/S12613-019-1767-Z
2. N. Bekoz and E. Oktay, The Role of Pore Wall Microstructure and Micropores on the Mechanical Properties of Cu-Ni-Mo Based Steel Foams, *Mater. Sci. Eng. A*, 2014, **612**, p 387–397
3. M. Salehi, S.M.H. Mirbagheri, and A. Jafari, Ramiani Experimental, Theoretical, and Numerical Investigations into the Compressive Behavior of Multi-Layer Metallic Foam Filled Tubes, *J. Mater. Eng. Perform.*, 2022, **31**(5), p 3723–3740. https://doi.org/10.1007/S11665-021-06475-9/FIGURES/17
4. A.A.A. John, S.S. Karibeeran, and P. Natarajan, Design and Analysis of Topologically Ordered Open-Cell Metal Foams by Rapid Manufacturing, *J. Mater. Eng. Perform.*, 2021, **30**(9), p 6549–6556. https://doi.org/10.1007/S11665-021-05906-X/FIGURES/10
5. C.M. Hsu, Y.C. Tzeng, S.F. Chen, Y.L. Chen, and H.L. Lee, Fabrication of 17–4PH Stainless Steel Foam by a Pressureless Powder Space Holder Technique, *Adv. Eng. Mater.*, 2021, **23**(6), p 2001202. https://doi.org/10.1002/ADEM.202001202
6. M. Yeganeh, M.T. Shoushtari, P. Jalali, T.S. Mohammadreza, and P.J. Affiliations, Evaluation of the Corrosion Performance of Selective Laser Melted 17–4 Precipitation Hardening Stainless Steel in Ringer's Solution, *J. Laser Appl.*, 2021, **33**(4), p 042001. https://doi.org/10.2351/7.0000445
7. M.B. Sedelnikova, Y.P. Sharkeev, T.V. Tolkacheva, P.V. Uvarkin, V.V. Chebodaeva, K.A. Prosolov, O.V. Bakina, A.D. Kashin, N.A. Shcheglova, A.A. Panchenko, I.B. Krasovsky, M.V. Solomatina, M.V. Efimenko, V.V. Pavlov, L.A. Cherdantseva, and I.A. Kirilova, Additively Manufactured Porous Titanium 3D–Scaffolds with Antibacterial Zn-, Ag- Calcium Phosphate Biocoatings, *Mater. Charact.*, 2022, **186**, p 111782
8. H.Ö. Gülsoy and R.M. German, Sintered Foams from Precipitation Hardened Stainless Steel Powder, *Powder Metall.*, 2013, **51**(4), p 350–353. https://doi.org/10.1179/174329008X286703
9. S.V. Raj, L.J. Ghosn, B.A. Lerch, M. Hebsur, L.M. Cosgriff, and J. Fedor, Mechanical Properties of 17–4PH Stainless Steel Foam Panels, *Mater. Sci. Eng. A*, 2007, **456**(1–2), p 305–316
10. J.B. Min, L.J. Ghosn, and B.A. Lerch, A Study for Stainless Steel Fan Blade Design with Metal Foam Core, *J. Sandw. Struct. Mater.*, 2014, **17**(1), p 56–73. https://doi.org/10.1177/1099636214554181
11. M. Gauthier, A. Katz, A. Maison, C.V. Cojocaru, and F. Bernier, Effect of Hardening Heat Treatment on the Mechanical Properties of a 17–4PH Stainless Steel Foam, *MRS Adv.*, 2018, **3**(62), p 3655–3668. https://doi.org/10.1557/ADV.2018.614
12. E. Bemporad, F. Carassiti, A. Tata, G. Gallinaro, and M. Paris, EB/UV Treatment of Protective Coatings for Porous Materials, *Radiat. Phys. Chem.*, 2000, **57**(3–6), p 393–397
13. S.M. Mukhopadhyay, P. Joshi, S. Datta, and J. Macdaniel, Plasma Assisted Surface Coating of Porous Solids, *Appl. Surf. Sci.*, 2002, **201**(1–4), p 219–226
14. H. Jain, D.P. Mondal, G. Gupta, and R. Kumar, Silver Flowers Decorated Open Cell Stainless Steel Foam for Bone Scaffold Application, *Mater. Today Commun.*, 2023, **34**, p 105392. https://doi.org/10.1016/J.MTCOMM.2023.105392
15. D. Ionita, C. Ungureanu, and I. Demetrescu, Electrochemical and Antibacterial Performance of CoCrMo Alloy Coated with Hydroxyapatite or Silver Nanoparticles, *J. Mater. Eng. Perform.*, 2013, **22**(11), p 3584–3591. https://doi.org/10.1007/S11665-013-0653-5/TABLES/3
16. S. Karakuş, İ Albayrak, N.B. Üllen, M.A. Insel, and A. Kilislioğlu, Preparation, Characterization and Evaluation of a Novel CMC/Chitosan-α-Fe_2O_3 Nanoparticles-Coated 17–4 PH Stainless-Steel Foam, *Polym. Bull.*, 2022, **79**(6), p 4133–4151. https://doi.org/10.1007/S00289-021-03700-2/FIGURES/8
17. K. Ibrahim and Q. Ahsanulhaq, Sonochemical-Assisted In Situ Electrochemical Synthesis of Ag/α-Fe2O3/TiO2 Nanoarrays to Harness Energy from Photoelectrochemical Water Splitting, *ACS Sustain. Chem. Eng.*, 2018, **6**(9), p 11235–11245
18. M. Shahjahan, M.H. Rahman, M.S. Hossain, A. Khatun, H. Rahman, A. Islam, and A. Begum, Synthesis and Characterization of Silver Nanoparticles by Sol-Gel Technique Article in Nanoscience and Nanometrology, *Nanosci. Nanometrology*, 2017, **3**(1), p 34–39. https://doi.org/10.11648/j.nsnm.20170301.16
19. P.G. Jamkhande, N.W. Ghule, A.H. Bamer, and M.G. Kalaskar, Metal Nanoparticles Synthesis: An Overview on Methods of Preparation, Advantages and Disadvantages, and Applications, *J. Drug Deliv. Sci. Technol.*, 2019, **53**, p 101174

20. S. Soleimani, A. Jannesari, M. Yousefzadi, A. Ghaderi, and A. Shahdadi, Eco-Friendly Foul Release Coatings Based on a Novel Reduced Graphene Oxide/Ag Nanocomposite Prepared by a Green Synthesis Approach, *Prog. Org. Coatings*, 2021, **151**, p 106107
21. A. García-Quintero and M. Palencia, A Critical Analysis of Environmental Sustainability Metrics Applied to Green Synthesis of Nanomaterials and the Assessment of Environmental Risks Associated with the Nanotechnology, *Sci. Total Environ.*, 2021, **793**, p 148524
22. N. Madima, S.B. Mishra, and A.K. Mishra, Nanotechnology and Green Materials: Introduction, Fundamentals, and Applications, *Green Functionalized Nanomaterials for Environmental Applications*. Elsevier, 2022, p 3–19. https://doi.org/10.1016/B978-0-12-823137-1.00001-4
23. Z. Issaabadi, H. Arabi, H. Bazgir, and R. Dehghan, Green Approaches for Nanotechnology, *Green Functionalized Nanomaterials for Environmental Applications*. Elsevier, 2022, p 365–398. https://doi.org/10.1016/B978-0-12-823137-1.00014-2
24. M. Zhu, X. Li, L. Ge, Y. Zi, M. Qi, Y. Li, D. Li, and C. Mu, Green Synthesis of κ-Carrageenan@Ag Submicron-Particles with High Aqueous Stability, Robust Antibacterial Activity and Low Cytotoxicity, *Mater. Sci. Eng. C*, 2020, **106**, p 110185
25. G. Oza, A. Reyes-Calderón, A. Mewada, L.G. Arriaga, G.B. Cabrera, D.E. Luna, H.M.N. Iqbal, M. Sharon, and A. Sharma, Plant-Based Metal and Metal Alloy Nanoparticle Synthesis: A Comprehensive Mechanistic Approach, *J. Mater. Sci.*, 2019, **55**(4), p 1309–1330. https://doi.org/10.1007/S10853-019-04121-3
26. S. Karakuş Ed., *Sonochemical Reactions*, IntechOpen, 2020 https://doi.org/10.5772/intechopen.83195
27. M.A. Shenashen, S.A. El-Safty, E.A. Elshehy, M.A. Shenashen, S.A. El-Safty, and E.A. Elshehy, Synthesis, Morphological Control, and Properties of Silver Nanoparticles in Potential Applications, *Part. Part. Syst. Charact.*, 2014, **31**(3), p 293–316. https://doi.org/10.1002/PPSC.201300181
28. A. Santhosh, V. Theertha, P. Prakash, and S. Smitha Chandran, From Waste to a Value Added Product: Green Synthesis of Silver Nanoparticles from Onion Peels Together with Its Diverse Applications, *Mater. Today Proc.*, 2021, **46**, p 4460–4463
29. E.S. Al-Sheddi, N.N. Farshori, M.M. Al-Oqail, S.M. Al-Massarani, Q. Saquib, R. Wahab, J. Musarrat, A.A. Al-Khedhairy, and M.A. Siddiqui, Anticancer Potential of Green Synthesized Silver Nanoparticles Using Extract of Nepeta Deflersiana against Human Cervical Cancer Cells (HeLA), *Bioinorg. Chem. Appl.*, 2018, **20**(1), p 9390784
30. N.M. Alabdallah and M.M. Hasan, Plant-Based Green Synthesis of Silver Nanoparticles and Its Effective Role in Abiotic Stress Tolerance in Crop Plants, *Saudi J. Biol. Sci.*, 2021, **28**(10), p 5631–5639
31. Z.P. Qiao, M.Y. Wang, J.F. Liu, and Q.Z. Wang, Green Synthesis of Silver Nanoparticles Using a Novel Endophytic Fungus Letendraea Sp WZ07: Characterization and Evaluation of Antioxidant, Antibacterial and Catalytic Activities (3-in-1 System), *Inorg. Chem. Commun.*, 2022, **138**, p 109301
32. A. Alcudia, B. Begines, P. Rodriguez-Lejarraga, V. Greyer, V.C.F. Godinho, E. Pajuelo, and Y. Torres, Development of Porous Silver Nanoparticle/Polycaprolactone/Polyvinyl Alcohol Coatings for Prophylaxis in Titanium Interconnected Samples for Dental Implants, *Colloid Interface Sci. Commun.*, 2022, **48**, p 100621
33. V.P. Veeraraghavan, N.D. Periadurai, T. Karunakaran, S. Hussain, K.M. Surapaneni, and X. Jiao, Green Synthesis of Silver Nanoparticles from Aqueous Extract of Scutellaria Barbata and Coating on the Cotton Fabric for Antimicrobial Applications and Wound Healing Activity in Fibroblast Cells (L929), *Saudi J. Biol. Sci.*, 2021, **28**(7), p 3633–3640
34. S. Sehgal, J. Kumar, and Z.Z.Z. Nishtha, Involvement of Gold and Silver Nanoparticles in Lung Cancer Nanomedicines: A Review, *Mater. Today Proc.*, 2022 https://doi.org/10.1016/j.matpr.2022.04.199
35. S. Ahmad, S. Munir, N. Zeb, A. Ullah, B. Khan, J. Ali, M. Bilal, M. Omer, M. Alamzeb, S.M. Salman, and S. Ali, Green Nanotechnology: A Review on Green Synthesis of Silver Nanoparticles—an Ecofriendly Approach, *Int. J. Nanomedicine*, 2019, **14**, p 5087. https://doi.org/10.2147/IJN.S200254
36. M. Devi, S. Devi, V. Sharma, N. Rana, R.K. Bhatia, and A.K. Bhatt, Green Synthesis of Silver Nanoparticles Using Methanolic Fruit Extract of Aegle Marmelos and Their Antimicrobial Potential against Human Bacterial Pathogens, *J. Tradit. Complement. Med.*, 2020, **10**(2), p 158–165
37. G. Karabulut, N. Beköz Üllen, E. Akyüz, and S. Karakuş, Surface Modification of 316L Stainless Steel with Multifunctional Locust Gum/Polyethylene Glycol-Silver Nanoparticles Using Different Coating Methods, *Prog. Org. Coatings*, 2023, **174**, p 107291
38. M.M. Solomon, S.A. Umoren, A.U. Israel, and E.E. Ebenso, Polypropylene Glycol-Silver Nanoparticle Composites: A Novel Anticorrosion Material for Aluminum in Acid Medium, *J. Mater. Eng. Perform.*, 2015, **24**(11), p 4206–4218. https://doi.org/10.1007/S11665-015-1716-6/FIGURES/11
39. A. Sharonova, K. Loza, M. Surmeneva, R. Surmenev, O. Prymak, and M. Epple, Synthesis of Positively and Negatively Charged Silver Nanoparticles and Their Deposition on the Surface of Titanium, *IOP Conf. Ser. Mater. Sci. Eng.*, 2016, **116**(1), p 012009. https://doi.org/10.1088/1757-899X/116/1/012009
40. R.K. Das and M. Das, Study of Silver Nanoparticle/Polyvinyl Alcohol Nanocomposite, *Int. J. Plast. Technol.*, 2019, **23**(1), p 101–109. https://doi.org/10.1007/S12588-019-09229-4/FIGURES/8
41. K. Guzmán, B. Kumar, M.J. Vallejo, M. Grijalva, A. Debut, and L. Cumbal, Ultrasound-Assisted Synthesis and Antibacterial Activity of Gallic Acid-Chitosan Modified Silver Nanoparticles, *Prog. Org. Coatings*, 2019, **129**, p 229–235
42. S.K. Das, S. Behera, J.K. Patra, and H. Thatoi, Green Synthesis of Sliver Nanoparticles Using Avicennia Officinalis and Xylocarpus Granatum Extracts and In Vitro Evaluation of Antioxidant, Antidiabetic and Anti-Inflammatory Activities, *J. Clust. Sci.*, 2019, **30**(4), p 1103–1113. https://doi.org/10.1007/S10876-019-01571-2
43. M.A. Hossain, B. Paul, K.A. Khan, M. Paul, M.A. Mamun, and M.E. Quayum, Green Synthesis and Characterization of Silver Nanoparticles by Using Bryophyllum Pinnatum and the Evaluation of Its Power Generation Activities on Bio-Electrochemical Cell, *Mater. Chem. Phys.*, 2022, **282**, p 125943
44. Jean M. Bokelmann, Maca (Lepidium Meyenii), *Medicinal Herbs in Primary Care*. Elsevier, 2022, p 489–493. https://doi.org/10.1016/B978-0-323-84676-9.00060-X
45. T.M. Silva, D.S. Fracasso, A.P. Vargas Visentin, C. Cassini, F.J. Scariot, S. Danetti, S. Echeverrigaray, S. Moura, L.B. Touguinha, C.S. Branco, and M. Salvador, Dual Effect of the Herbal Matcha Green Tea (Camellia Sinensis L. Kuntze) Supplement in EA.Hy926 Endothelial Cells and Artemia Salina, *J. Ethnopharmacol.*, 2022, **298**, p 115564. https://doi.org/10.1016/J.JEP.2022.115564
46. F.M. Rezaeian and B.F. Zimmermann, Simplified Analysis of Flavanols in Matcha Tea, *Food Chem.*, 2022, **373**, p 131628
47. E. Tan, İM. Kahyaoğlu, and S. Karakuş, A Sensitive and Smartphone Colorimetric Assay for the Detection of Hydrogen Peroxide Based on Antibacterial and Antifungal Matcha Extract Silver Nanoparticles Enriched with Polyphenol, *Polym. Bull.*, 2021, **38**, p 1–27
48. S. Karakuş, G. Baytemir, and N. Taşaltın, Digital Colorimetric and Non-Enzymatic Biosensor with Nanoarchitectonics of Lepidium Meyenii-Silver Nanoparticles and Cotton Fabric: Real-Time Monitoring of Milk Freshness, *Appl. Phys. A Mater. Sci. Process.*, 2022, **128**(5), p 1–11. https://doi.org/10.1007/S00339-022-05529-6/FIGURES/10
49. C.A. Acevedo, D.A. López, M.J. Tapia, J. Enrione, O. Skurtys, F. Pedreschi, D.I. Brown, W. Creixell, and F. Osorio, Using RGB Image Processing for Designing an Alginate Edible Film, *Food Bioprocess Technol.*, 2012, **5**(5), p 1511–1520. https://doi.org/10.1007/S11947-010-0453-Y/TABLES/2
50. L. Gutin, Equating Color and Transparency, 2014, https://www.viget.com/articles/equating-color-and-transparency/. Accessed 19 June 2022
51. R. Houhou and T. Bocklitz, Trends in Artificial Intelligence, Machine Learning, and Chemometrics Applied to Chemical Data, *Anal. Sci. Adv.*, 2021, **2**(3–4), p 128–141. https://doi.org/10.1002/ANSA.202000162
52. Y. Iida, K. Watanabe, Y. Ominami, T. Toyoguchi, T. Murayama, and M. Honda, Development of Rapid and Highly Accurate Method to Measure Concentration of Fibers in Atmosphere Using Artificial Intelligence and Scanning Electron Microscopy, *J. Occup. Health*, 2021, **63**(1), p e12238. https://doi.org/10.1002/1348-9585.12238
53. A.G. Okunev, M. Yu Mashukov, N.N. Sankova, A.V. Nartova, and A.V. Matveev, Artificial Intelligence for Imaging Data Analysis in Materials Science: Microscopy and Behind, *IOP Conf. Ser. Mater. Sci.*

Eng., 2021, **1155**(1), p 012015. https://doi.org/10.1088/1757-899X/1155/1/012015
54. S. Ragi, M.H. Rahman, J. Duckworth, J. Kalimuthu, P. Chundi, and V. Gadhamshetty, Artificial Intelligence-Driven Image Analysis of Bacterial Cells and Biofilms, *IEEE/ACM Trans. Comput. Biol. Bioinforma.* 2021
55. M. Gomathi, P.V. Rajkumar, A. Prakasam, and K. Ravichandran, Green Synthesis of Silver Nanoparticles Using Datura Stramonium Leaf Extract and Assessment of Their Antibacterial Activity, *Resour. Technol.*, 2017, **3**(3), p 280–284
56. Y. Kim, V.R. Babu, D.T. Thangadurai, K.S.V. Krishna Rao, H. Cha, C. Kim, W. Joo, and Y.-I. Lee, Synthesis, Characterization, and Antibacterial Applications of Novel Copolymeric Silver Nanocomposite Hydrogels, *Bull. Korean Chem. Soc*, 2011, **32**(2), p 553
57. I.A. Aminatun, D.H. Furqon, and C.A.C. Abdullah, Antibacterial Properties of Silver Nanoparticle (AgNPs) on Stainless Steel 316L, *Nanomedicine Res. J.*, 2021, **6**(2), p 117–127
58. K. Mallikarjuna, N. John Sushma, G. Narasimha, L. Manoj, and B. Deva Prasad Raju, Phytochemical Fabrication and Characterization of Silver Nanoparticles by Using Pepper Leaf Broth, *Arab. J. Chem.*, 2014, **7**(6), p 1099–1103. https://doi.org/10.1016/J.ARABJC.2012.04.001
59. S.A.M. Gowda, L.C. Goveas, and K. Dakshayini, Adsorption of Methylene Blue by Silver Nanoparticles Synthesized from Urena Lobata Leaf Extract: Kinetics and Equilibrium Analysis, *Mater. Chem. Phys.*, 2022, **288**, p 126431
60. A. Trybala and V. Starov, Kinetics of Spreading Wetting of Blood over Porous Substrates, *Curr. Opin. Colloid Interface Sci.*, 2018, **36**, p 84–89
61. J. Anthony von Fraunhofer, Adhesion and Cohesion, *Int. J. Dent.*, 2012, **2012**, p 1–8. https://doi.org/10.1155/2012/951324
62. R.S. Kühnel, S. Obeidi, M. Lübke, A. Lex-Balducci, and A. Balducci, Evaluation of the Wetting Time of Porous Electrodes in Electrolytic Solutions Containing Ionic Liquid, *J. Appl. Electrochem.*, 2013, **43**(7), p 697–704. https://doi.org/10.1007/S10800-013-0558-X/FIGURES/4
63. P. Estellé, D. Cabaleiro, G. Żyła, L. Lugo, and S.M.S. Murshed, Current Trends in Surface Tension and Wetting Behavior of Nanofluids, *Renew. Sustain. Energy Rev. Pergamon*, 2018, **94**, p 931–944
64. J. Wu, N. Wang, L. Wang, H. Dong, Y. Zhao, and L. Jiang, Electrospun Porous Structure Fibrous Film with High Oil Adsorption Capacity, *ACS Appl. Mater. Interfaces.*, 2012, **4**(6), p 3207–3212. https://doi.org/10.1021/AM300544D/ASSET/IMAGES/MEDIUM/AM-2012-00544D_0005.GIF
65. N. Bekoz and E. Oktay, Effects of Carbamide Shape and Content on Processing and Properties of Steel Foams, *J. Mater. Process. Technol.*, 2012, **212**(10), p 2109–2116
66. K. Jeeva Jothi, S. Balachandran, and K. Palanivelu, Synergistic Combination of Phyllanthus Niruri/Silver Nanoparticles for Anticorrosive Application, *Mater. Chem. Phys.*, 2022, **279**, p 125794. https://doi.org/10.1016/J.MATCHEMPHYS.2022.125794
67. A. Panáček, L. Kvítek, R. Prucek, M. Kolář, R. Večeřová, N. Pizúrová, V.K. Sharma, T. Nevěčná, and R. Zbořil, Silver Colloid Nanoparticles: Synthesis, Characterization, and Their Antibacterial Activity, *J. Phys. Chem. B*, 2006, **110**(33), p 16248–16253. https://doi.org/10.1021/JP063826H/SUPPL_FILE/JP063826HSI20060619_085949.PDF
68. S. Calderon Velasco, A. Cavaleiro, and S. Carvalho, Functional Properties of Ceramic-Ag Nanocomposite Coatings Produced by Magnetron Sputtering, *Prog. Mater. Sci.*, 2016, **84**, p 158–191
69. M. Soloviev and A. Gedanken, Coating a Stainless Steel Plate with Silver Nanoparticles by the Sonochemical Method, *Ultrason. Sonochem.*, 2011, **18**(1), p 356–362
70. M. Şahin and İH. Gübbük, Antioksidan Gümüş Nanoparçacıkların Sentezlenmesi, Karakterizasyonu ve Kataliz Uygulamaları, *Int. J. Adv. Eng. Pure Sci.*, 2019, **31**, p 75–83. https://doi.org/10.7240/JEPS.497405
71. M.F. Ashby, "Metal Foams: A Design Guide," Butterworth-Heinemann, 2000
72. I. Mutlu and E. Oktay, Characterization of 17–4 PH Stainless Steel Foam for Biomedical Applications in Simulated Body Fluid and Artificial Saliva Environments, *Mater. Sci. Eng. C*, 2013, **33**(3), p 1125–1131
73. N. Bekoz and E. Oktay, Mechanical Properties of Low Alloy Steel Foams: Dependency on Porosity and Pore Size, *Mater. Sci. Eng. A*, 2013, **576**, p 82–90
74. A.D. Preston and K. Ma, Insight into the Effects of Pore Size and Distribution on Mechanical Properties of Austenite Stainless Steels, *J. Mater. Sci.*, 2021, **56**(30), p 17278–17295. https://doi.org/10.1007/S10853-021-06363-6/TABLES/3
75. K.A. Hing, S. Saeed, B. Annaz, T. Buckland, and P.A. Revell, Microporosity Affects Bioactivity of Macroporous Hydroxyapatite Bone Graft Substitutes, *Key Eng. Mater.*, 2004, **254–256**, p 273–276. https://doi.org/10.4028/WWW.SCIENTIFIC.NET/KEM.254-256.273
76. I.O. Smith, F. Ren, M.J. Baumann, and E.D. Case, Confocal Laser Scanning Microscopy as a Tool for Imaging Cancellous Bone, *J. Biomed. Mater. Res. B. Appl. Biomater.*, 2006, **79**(1), p 185–192. https://doi.org/10.1002/JBM.B.30529
77. T. Kokubo, *Bioceramics and Their Clinical Applications*, Woodhead Publishing Limited, 2008. https://doi.org/10.1533/9781845694227
78. L. Müller and F.A. Müller, Preparation of SBF with Different HCO3- Content and Its Influence on the Composition of Biomimetic Apatites, *Acta Biomater.*, 2006, **2**(2), p 181–189. https://doi.org/10.1016/J.ACTBIO.2005.11.001
79. L. Wang, J.F. Su, and X. Nie, Corrosion and Tribological Properties and Impact Fatigue Behaviors of TiN- and DLC-Coated Stainless Steels in a Simulated Body Fluid Environment, *Surf. Coatings Technol.*, 2010, **205**(5), p 1599–1605
80. S. Mine, G. Sugerman, and E.C. Frey, Effects of Surface Characteristics on the in Vitro Biocompatibility Response of Niti Shape Memory Alloys, *Acad. Platf. J. Eng. Sci.*, 2019, **7**(2), p 285–290. https://doi.org/10.21541/APJES.461169
81. C. Wu, M. Chen, T. Zheng, and X. Yang, Effect of Surface Roughness on the Initial Response of MC3T3-E1 Cells Cultured on Polished Titanium Alloy, *Biomed. Mater. Eng.*, 2015, **26**(s1), p S155–S164
82. H. Al-Turaif, D.W. Bousfield, and P. LePoutre, The Influence of Substrate Absorbency on Coating Surface Chemistry, *Prog. Org. Coatings*, 2002, **44**(4), p 307–315
83. T.C. Lim, K.S. Chian, and K.F. Leong, Cryogenic Prototyping of Chitosan Scaffolds with Controlled Micro and Macro Architecture and Their Effect on in Vivo Neo-Vascularization and Cellular Infiltration, *J. Biomed. Mater. Res. A*, 2010, **94**(4), p 1303–1311. https://doi.org/10.1002/JBM.A.32747
84. R. Alias, R. Mahmoodian, and M.H. Abd Shukor, Development and Characterization of a Multilayer Silver/Silver-Tantalum Oxide Thin Film Coating on Stainless Steel for Biomedical Applications, *Int. J. Adhes. Adhes.*, 2019, **92**, p 89–98
85. A. Başargan, "Bakırın Elektrospark Mikroalaşımlandırma Yöntemi Ile Gümüşle Kaplanması," 2010, https://acikbilim.yok.gov.tr/handle/20.500.12812/620397. Accessed 22 June 2022
86. A. Santos-Coquillat, E. Martínez-Campos, H. Mora Sánchez, L. Moreno, R. Arrabal, M. Mohedano, A. Gallardo, J. Rodríguez-Hernández, and E. Matykina, Hybrid Functionalized Coatings on Metallic Biomaterials for Tissue Engineering, *Surf. Coatings Technol.*, 2021, **422**, p 127508
87. M.H. Sarrafzadeh, H.J. La, J.Y. Lee, D.H. Cho, S.Y. Shin, W.J. Kim, and H.M. Oh, Microalgae Biomass Quantification by Digital Image Processing and RGB Color Analysis, *J. Appl. Phycol.*, 2015, **27**(1), p 205–209. https://doi.org/10.1007/S10811-014-0285-7/FIGURES/5
88. T. Wang, L. Wang, Q. Lu, and Z. Fan, Influence of Anodized Titanium Abutments on the Esthetics of the Peri-Implant Soft Tissue: A Clinical Study, *J. Prosthet. Dent.*, 2021, **125**(3), p 445–452
89. D.Ö. Dede, A. Armağanci, G. Ceylan, E. Celik, S. Cankaya, and B. Yilmaz, Influence of Implant Abutment Material on the Color of Different Ceramic Crown Systems, *J. Prosthet. Dent.*, 2016, **116**(5), p 764–769
90. K. Ahn, S. Han, K. Yun, W. Lee, D.G. Lee, S.M. Kang, Y.B. Choi, K. Han, and Y.J. Ahn, A Real-Time Detection Device for the Rapid Quantification of Skin Casual Sebum Using the Oil Red O Staining Method, *Sensors.*, 2022, **22**(8), p 3016. https://doi.org/10.3390/S22083016
91. V.C.. B.K. Malshe, Infrared Reflective Inorganic Pigments: Ingenta Connect, *Recent Patents Chem. Eng.* 2008, **1**(1), p 67–79, https://www.

ingentaconnect.com/content/ben/cheng/2008/00000001/00000001/art00006. Accessed 24 June 2022
92. T. Watson, C. Charbonneau, D. Bryant, and D. Worsley, Acid Treatment of Titania Pastes to Create Scattering Layers in Dye-Sensitized Solar Cells, *Int. J. Photoenergy*, 2012, **2012**, p 1–8
93. J.W. Huang, W.C. Chen, T.K. Huang, P.S. Fu, P.L. Lai, C.F. Tsai, and C.C. Hung, Using a Spectrophotometric Study of Human Gingival Colour Distribution to Develop a Shade Guide, *J. Dent.*, 2011, **39**(SUPPL. 3), p e11–e16
94. O. Ginesin, H. Zigdon-Giladi, E. Gabay, E.E. Machtei, E. Mijiritsky, and Y. Mayer, Digital Photometric Analysis of Gingival Response to Periodontal Treatment, *J. Dent.*, 2022, **127**, p 104331

Publisher's Note Springer Nature remains neutral with regard to jurisdictional claims in published maps and institutional affiliations.

Springer Nature or its licensor (e.g. a society or other partner) holds exclusive rights to this article under a publishing agreement with the author(s) or other rightsholder(s); author self-archiving of the accepted manuscript version of this article is solely governed by the terms of such publishing agreement and applicable law.